2015

Pressurized Metal Bellows Shock Absorber for Space Applications.

John Trautwein
University of Central Florida

PRESSURIZED METAL BELLOWS SHOCK ABSORBER FOR SPACE APPLICATIONS

by

JOHN TRAUTWEIN
B.S. Rutgers University, 1996
B.S. Florida State University, 2004

A thesis submitted in partial fulfilment of the requirements
for the degree of Master of Science
in the Department of Mechanical and Aerospace Engineering
in the College of Engineering & Computer Science
at the University of Central Florida
Orlando, Florida

Fall Term
2015

Major Professor: Jeffrey L. Kauffman

ABSTRACT

Numerous spacecraft designs exist for exploring the surfaces of planetary bodies and each have their own advantages and disadvantages. All successful landings have been made by stationary landers or wheeled rovers that rely on one-time use mechanisms, such as crushable aluminum honeycomb shock absorbers or inflatable airbags, to reduce shock loading to the spacecraft during landing. The stationary lander is the simplest type of lander, but can only take data from one location. Wheeled rovers add complexity in exchange for mobility to explore different locations. Rovers are limited by the terrain they can traverse; rovers becoming stuck have ended missions. In contrast to rovers and stationary landers, hoppers explore by making multiple launch and landing hops. They have the advantage of being able to avoid terrain that would cause a rover to become stuck. A hopper may require a landing shock absorber that can reliably operate multiple times in harsh environments.

Most terrestrial shock absorbers use hydraulic fluid, allowing for compact and inexpensive devices. Hydraulics have been used in space applications, but require thermal controls to maintain the proper fluid viscosity. They also require dynamic seals which, in the case of a leak, can degrade performance, shorten mission life, and contaminate sensitive science equipment. Leakage is also a concern in pressurized systems in space because missions can take decades from when a system is installed to when it actually is used.

To address these issues, a pressurized metal bellows shock absorber is proposed. This shock absorber could operate at nearly any expected spacecraft environment. Metal bellows are designed to operate from cryogenic temperatures to several hundred degrees Celsius. A hermetically sealed system eliminates the risks of a system with seals. Metal bellows are in common use for terrestrial harsh environments and vacuum applications. Small metal bellows are used as dampers for

pressure control systems with small displacements.

Models for the dynamics of this device are developed and presented here. Starting from the ideal gas law, polytropic compression, and compressible flow through an orifice, differential equations of motion and pressure are derived. These equations are nonlinear for the displacements under consideration and are nondimensionalized to help provide insight. Equations for static equilibrium, maximum initial displacement bounds, and estimated natural frequency are presented.

Metal bellows can operate as a passive damper with a simple orifice between the control volumes. Optimization is performed for the nondimensional model of a passive damper. Because the response is highly nonlinear, a method is developed to estimate a damping coefficient that is used as the objective function for this optimization. Feasibility of this concept is investigated through an example design problem using data from a metal bellows manufacturer as constraints. An optimal mass configuration is found that meets the design constraints.

Performance can be improved over the passive system by adding control. The first control strategy involves a check valve, such that the effective orifice size varies between compression and extension. The next control strategy replaces the orifice with a control valve. Varying the valve opening and closing timing can achieve optimal performance. Finally, using the metal bellows as an actuator to help launch the hopper is investigated. While the valve is closed, the gas in the second volume is compressed. Then the valve is opened the hopper is launched.

The results of this research show that a metal bellows device holds promise as a landing shock absorber and launch actuator to extend the range of hopper spacecraft.

ACKNOWLEDGMENTS

I would like to thank my graduate adviser Jefferey L. Kauffman for his guidance and patience during my journey through graduate school and this research. He always seems to provide just enough direction to keep me from getting hopelessly lost but the freedom to explore this topic. I would also like to thank Joette Feeney from Kennedy Space Center for selecting me for the Kennedy Space Center Graduate Fellowship Program which provided the funding for my Master's Degree and my supervisors Todd Steinrock and Ned Voska for allowing the flexibility to juggle work and school responsibilities. I appreciate all of the help from my coworkers at the NASA Prototype Laboratory for putting up with what must seem to be a random schedule for the past two and a half years. Finally I could not have done this without the support of my loving wife Ileana and my children Robert, Victoria, and Thomas. We have spent many nights together around the kitchen table on our schoolwork and this thesis is the culmination of these efforts.

TABLE OF CONTENTS

LIST OF FIGURES

LIST OF TABLES

CHAPTER 1: INTRODUCTION

1.1 Hopper Spacecraft

Exploring planetary bodies in our solar system is important for many reasons. Each body provides it own laboratory to test theories on planet formation and biological evolution. Exploring small bodies such as comets and asteroids allows us to travel back in time; geologic processes happen much slower without the weathering found on Earth. Learning about these bodies can have practical benefits, the most important being how to redirect them if they are on a collision course with Earth.

A hopper explores the surface of planetary bodies using a hopping motion, in contrast to traditional rovers. A rover has the advantage of being able to accurately position the vehicle at points of interest and move methodically over terrain. Roving works well if the location being explored is relatively flat and free of obstacles and has sufficient gravity to give the rover wheels traction. In contrast, a hopper is able to explore terrain a rover cannot. For example a hopper could scale large cliffs or hop into a crater and then hop back out. Indeed, Mars' Bonneville crater was not explored because of risk to the rover [2]. A hopper does not rely solely on traction and is less likely to get stuck in loose soil, which is what led to the end of mission for the MER-A Rover Spirit [3]. Finally, hopping is better than roving on bodies like asteroids, comets, dwarf planets, or small moons, where the low gravity provides insufficient wheel traction.

Proposed mechanisms for hopping include springs, reaction wheels, and propellant or cold gas thrusters. Some hopper are designed to crash land on very low gravity bodies and, once they bounce and roll to a stop, reorient themselves to take measurements and prepare for the next hop. Others use thrusters and soft land using shock absorbing landing gear. While preferable from

a structural standpoint this requires longer thruster firing and thus consumes more fuel, limiting mission life.

A pressurized metal bellows shock absorber is proposed as a way of increasing hopper range. Metal bellows can be used as a shock absorber during landing as well as to initiate a hop. Because the metal bellows is hermetically sealed, no gas is lost during use. The shock absorber could be designed to function as a spring with no damping, allowing the craft to travel by consecutive hops without using any fuel, terrain permitting, thereby reserving the thrusters for extreme circumstances.

1.2 Shock Absorbers and Damping Mechanisms

Shock absorbers combine a spring and a damper to arrest motion. The spring allows the system to oscillate around static equilibrium, while the damper converts the energy of motion to another form of energy, such as heat and pressure. A typical hydraulic shock absorber is shown in Figure 1.1. Hydraulic shock absorbers are composed of piston submersed in hydraulic fluid. As the device strokes, the fluid, typically assumed to be incompressible, is pushed between two reservoirs through an orifice. The back pressure is a function of flow velocity, resulting in damping. Because the piston rod displaces fluid as it enters the fluid reservoir, the fluid compresses the gas in the bottom reservoir, which provides a pressure force. Hydraulic shock absorbers are used in terrestrial applications such as airplane landing gears, automotive suspensions, and machine isolation because of their compactness and reliability.

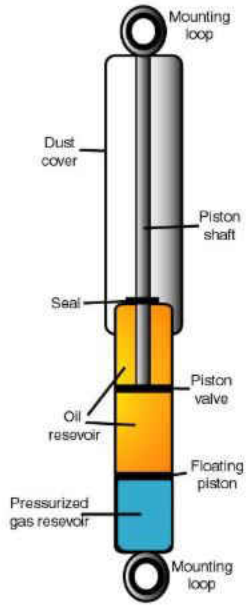

Figure 1.1: Hydraulic Shock Absorber Schematic [4]

Gas is typically not used as the working fluid in shock absorbers because the compressibility of the gas requires a significant amount of motion before any damping occurs, which complicates the dynamic analysis. Any gas remaining in the piston volume acts as a spring, sending energy back into the system, causing oscillations. A passive gas damper can be designed to minimize oscillation, but only for particular initial conditions. During a mission a hopper with thrusters will expend propellant and lose mass, and it will impact at different speeds. An adaptive system is required to minimize the bounce for these variable conditions.

For a hopper spacecraft, the compressibility of the gas can be exploited. For example, a valve could replace the orifice and be kept closed while the pressure in the second volume increased. Then by opening the valve the pressure on the bellows would launch the craft. By keeping the valve closed, at impact, the metal bellows would act like a spring allowing consecutive hops.

1.3 Metal Bellows Shock Absorber

Metal bellows actuators are a standard product used when a hermetically sealed actuator is required, typically in a clean room or vacuum chamber. First, the bellows are formed from individual stamped metal diaphragms (Figure 1.2a). Two diaphragms are welded together to make a convolution (Figure 1.2b). Then, the convolutions are stacked and welded together to form a complete bellows (Figure 1.2c). Finally, the bellows are welded into the actuator housing (Figure 1.2d).

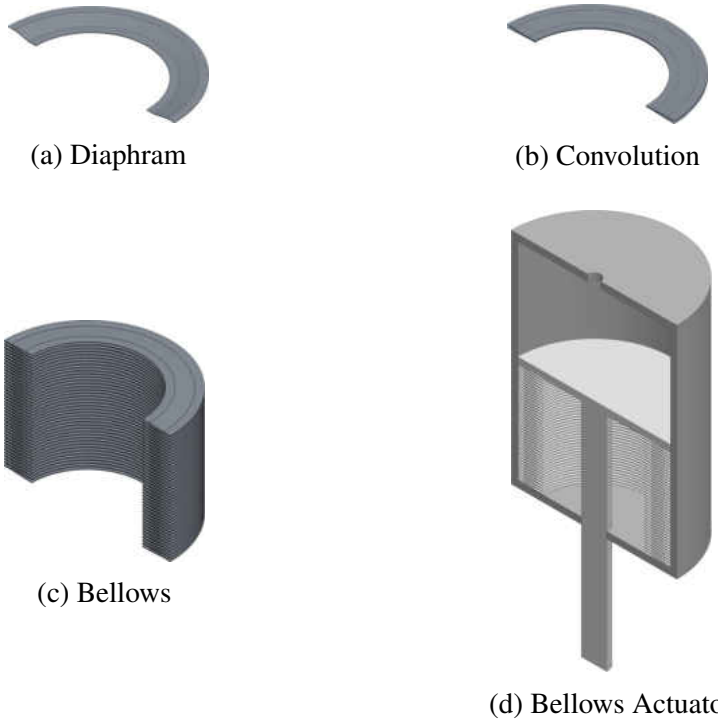

(a) Diaphram

(b) Convolution

(c) Bellows

(d) Bellows Actuator

Figure 1.2: Metal Bellows Actuator Construction

The proposed metal bellows shock absorber modifies a metal bellows actuator by adding a second volume connected to the first through an orifice as shown in Figure 1.3. Metal bellows are well suited to be used as landing shock absorbers. The extreme thermal environment that a lander

would experience requires hydraulic shock absorbers to have active thermal management to maintain the required viscosity. Spacecraft thermal management requires power and mass allocations; metal bellows would not require active thermal management, so would reduce power and mass of the system. Furthermore, dynamic seals are problematic in the electrostatically charged dusty environments found on most small planetary bodies. The dust is very abrasive and tends to stick to surfaces causing seals to degrade and leak. Subsystems on spacecraft can be left unused for more than a decade waiting for launch and during transit, requiring very small leak rates to ensure sufficient gas remains when needed. In addition, seals can stick and fail to move after sitting for long durations in harsh conditions. In contrast, hermetically sealed metal bellows eliminate these problems.

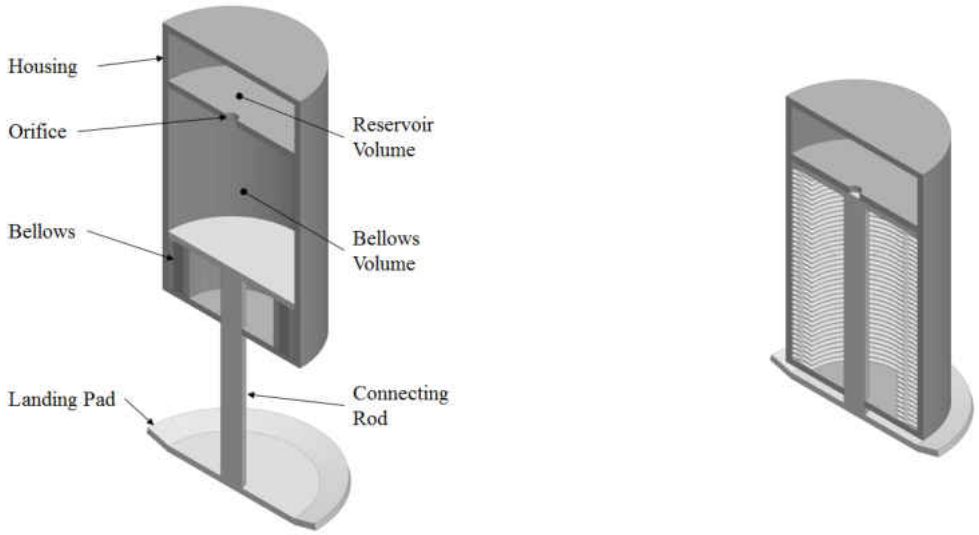

(a) Extended

(b) Retracted

Figure 1.3: Metal Bellows Shock Absorber

1.4 Motivation

The motivation of this research is to investigate the feasibility of using metal bellows to extend the range of hopper spacecraft. As a first effort in this investigation, the hopper is simplified as a single degree of freedom system with the mass directly coupled to the shock absorber constrained to vertical movement. On a real spacecraft the metal bellows would most likely be a component in a landing gear, but the methods developed here should prove feasibility and provide a guide regardless of the particular implementation.

The analysis starts by calculating the effective area for a metal bellows and comparing the effective area to what the metal bellows industry uses. The differential equations of motion and pressure are derived and normalized. Equations for static equilibrium solution, maximum initial displacement bounds, and estimated natural frequency are presented. Then the input parameters to the nondimensional model are varied around a set of initial parameters to see how the response changes. The various responses provides considerable insight into the system with the acknowledgment that the system is highly nonlinear and variations around one location are not assured to be general. A method is developed to estimate a linear damping ratio that is used as the objective function for optimization.

Metal bellows can operate as a passive damper with a simple orifice between the control volumes as shown in Figure 1.4. Optimization is performed for the nondimensional model of a passive damper. Feasibility of this concept is investigated through an example design problem using data from a metal bellows manufacturer as constraints. An optimal configuration is found that meets the design constraints.

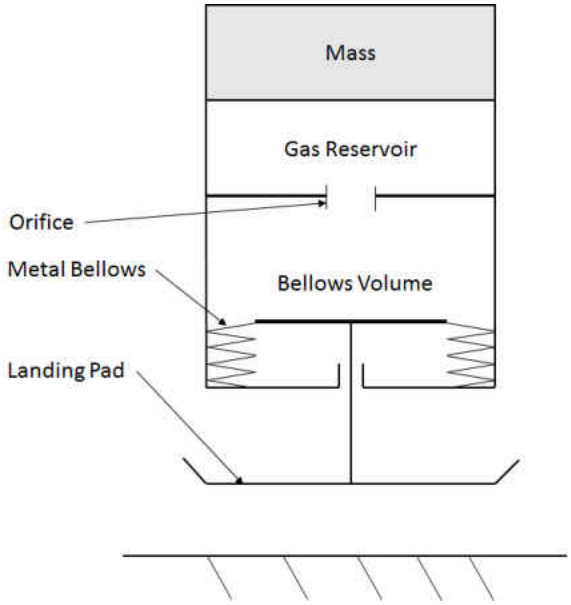

Figure 1.4: Metal Bellows Shock Absorber Schematic

Performance can be improved over the passive system by adding controls. The first control strategy is adding a check valve to control the effective orifice size for the compression and extension stroke. The next control strategy replaces the orifice with a control valve and by timing the opening and closing of the valve, optimal performance can be achieved. Finally, the concept of compressing the gas in the second volume is proposed so that, in combination with the control valve, the metal bellows can be used to help launch the hopper.

1.5 Goals for Current Research

The primary goal of this research is to prove the feasibility of using pressurized metal bellows shock absorber for a hopper spacecraft. It would act as a shock absorber on landing and can initiate hops without using propellant, which could give a hopper essentially unlimited range. This

device would be hermetically sealed and capable of operating in harsh environmental conditions for extended mission durations without leaking or sticking. Active controls could be implemented to provide the shock absorption required for landing on low gravity bodies.

The secondary goal is to provide a future hopper spacecraft designer with the theoretical background, analysis, and tools required to design this device. The sensitivity of the response to the variation of input parameters is discussed, optimization techniques are presented, and control systems are proposed and evaluated. This analysis should give a designer a firm base from which to move forward with implementation.

CHAPTER 2: LITERATURE REVIEW

There is a large volume of research on shock absorbers and damping mechanisms that seems to cluster by configuration. The first configuration is isolating a vibrating mass from the base, such as for rotating machine supports. Another configuration is isolating a mass from base excitation, such as for vehicle suspensions or building seismic isolation. Finally, there are impact absorbing cases, such as airplane landing gear designs. The majority of the research I found was for the first two cases which provided excellent examples for the model development and nondimensionalization methodology used in this analysis. The impact absorbing cases either used hydraulics which is not relevant here or those that did used pneumatic systems did not describe the models or used linearization for small displacements. In addition, lander and hopper spacecraft were investigated to evaluate landing mechanisms. While not immediately helpful in developing a model, they were useful to determine the environmental and mission parameters such as gravity, vehicle mass, and impact velocities for the target planetary bodies. Finally, research into the metal bellows industry was conducted to see how these devices are typically designed and fabricated.

2.1 Planetary Landers and Hoppers

Many spacecraft have landed successfully. Several hopper spacecrafts have been proposed, and some have even launched, but none have been been successfully landed. A summary of the planetary lander mission data is shown in Table 2.1.

2.1.1 Apollo

Since the Apollo Lunar Module (LM) only landed once during the mission it used a crushable Aluminum honeycomb impact absorber as shown in Figure 2.1 [5,6]. Because it takes a constant force to crush the honeycomb through its entire stroke, the force displacement curve is a rectangular profile and it absorbs the maximum energy for a given stroke and maximum allowable deceleration. The landing data estimated that 60% of the landing energy was absorbed by the footpads compressing the regolith.

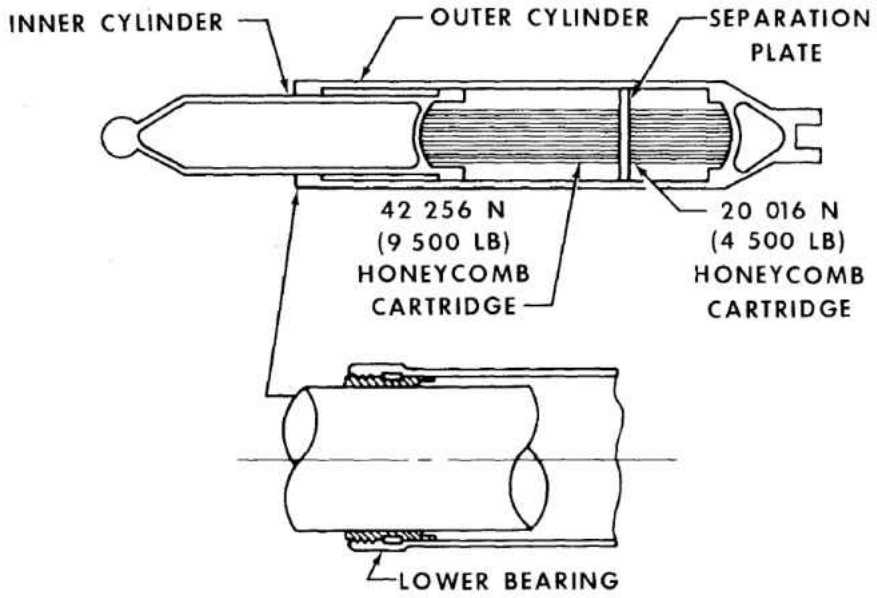

Figure 2.1: Apollo Lunar Module Landing Gear Primary Strut. From [7]

2.1.2 PHOBOS

In 1988 and 1989 the former Soviet Union launched the two PHOBOS missions to study Mars and it's moons. PHOBOS 2 had a hopper named PROP-F to explore Mars' moon Phobos [8]. The

hopper is shown in Figure 2.2. The hopper was designed to launch itself in a particular direction using a compressed spring, then crash land and roll to a stop. Arms would extend to orient the hopper on its foot. Unfortunately the mission failed before the hopper could be deployed.

Figure 2.2: PROP-F. From [9]

2.1.3 Hayabusa

Japan's Space Agency (JAXA) launched the Hayabusa mission to return a sample from the Near Earth Asteroid 25143 Itokawa in 2003 [10]. This mission contained a minilander named MINERVA as seen in Figure 2.3. MINERVA was designed to hop over the surface of 25143 Itokawa by using two reaction wheels. One would rotate the vehicle to the desired direction and the second would cause the vehicle to rotate around its base launching it off the surface onto a ballistic trajectory. Unfortunately, this part of the mission failed when the hopper was released from the orbiting spacecraft with the incorrect velocity. Instead, it never made it to the surface of the asteroid and became solar satellite.

Figure 2.3: MINERVA. From [10]

2.1.4 Rosetta

The Rosetta mission launched in 2004. Ten years later it was inserted into orbit of the comet 67P/ Churyumov. In November of 2014, the Philae lander as shown in Figure 2.4 undocked from the Rosetta orbiter on a ballistic trajectory with the comet [11]. To land in the low gravity the lander was equipped with ice screws that would automatically screw into the surface upon impact. There was a damper between the main body of the lander and the landing feet, to decouple the rotation of the landing feet from the body. The lander also had thrusters and harpoons to attempt to force the lander onto the surface. In the end, the thrusters, harpoon, and ice screws failed to keep the lander on the surface. Philae inadvertently became the first hopper by bouncing at an estimated $4 \times 10^{-1}\,\mathrm{m\,s^{-1}}$ away from the surface. This first bounce lasted for 1 hour and 50 minutes and

covered approximately 1 km. During this bounce the data suggests that the lander hit the rim of a crater before coming to rest near a cliff. There has only been intermittent contact since the landing.

Figure 2.4: Philae Lander. From [12]

2.1.5 Talaris Planetary Hopper

Draper Laboratory is working on designing a Lunar hopper for the Google X-prize [13, 14]. Their design is using cold gas thrusters to perform the hopping maneuver. This type of system relies on expendable fuel which limits the range their hopper can explore. This type of hopper could benefit from using the proposed metal bellows shock absorber by allowing a higher landing speed and providing assistance initiating hops, thereby reducing fuel use.

Table 2.1: Planetary Lander Mission Data

Lander	Mass (kg)	Landing Velocity ($\mathrm{m\,s^{-1}}$)	Body	Surface Gravity ($\mathrm{m\,s^{-2}}$)	Escape Velocity ($\mathrm{m\,s^{-1}}$)
Lunar Module	7000	3	Moon	1.62	2380
PROP-F	45	2	Phobos	5.7×10^{-3}	11.39
MINERVA	5.9×10^{-1}	5×10^{-2}	25143 Itokawa	1×10^{-4}	2×10^{-1}
Philae	100	1	Comet 67P	1×10^{-3}	1

2.2 Shock Absorbers and Dampers

2.2.1 Hydraulic Shock Absorbers

The majority of research on hydraulic shock absorbers stems from their widespread use in terrestrial applications. Duym et al. compare analytical and empirical models of hydraulics shock absorbers [15]. Perhaps the closest application to the current project in space applications is Wang et at. proposing adaptive controls of magnetorheological hydraulics dampers to reduce structural vibration [16].

2.2.2 Pneumatic Cylinders

Wang et al. model the dynamics of a double acting pneumatic cylinder with pneumatic cushions [17,18]. Pneumatic cushions work by restricting the exit orifice area when the piston nears the end of stroke, thereby increasing back pressure, allowing the piston to slowly reach the end of stroke.

These types of cylinders are adjusted once installed for the particular load and impact speed by adjusting an exhaust valve. Maré et al. improves on this model by using ISO standards for flow through the orifice, not assuming an ideal gas, and and taking seal friction into account [19]. However, they were unable to predict seal friction in experiments because it changes as the seals degrade over time.

2.2.3 Linear Models for Gas Spring

Gas springs can also be used for vibration isolation. Most research concerning vibration isolation assumes small displacements in relation to the volume which allows the equations to be linearized for frequency analysis [20, 21]. Others investigate flow restrictions other than orifices such as capillary tubes and porous plugs [22, 23]. These papers provided context on the ways researchers analyze gas devices such as spring/dampers.

2.2.4 Nonlinear Models for Gas Spring

Andersen gives the equation for the nonlinear motion of a pneumatic spring mass system [1]; a full derivation follows. Starting with the diagram of the spring in Figure 2.5 and with the variables defined as shown in Table 2.2, the equation of motion is:

$$m\frac{\mathrm{d}^2x}{\mathrm{d}t^2} = (P_3 - P_2)\,A_p + mg \tag{2.1}$$

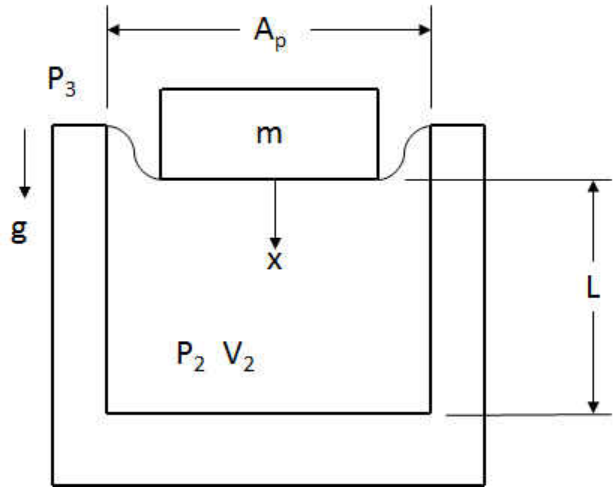

Figure 2.5: Nonlinear Pneumatic Mass/Spring. Reproduced from [1]

Table 2.2: Nonlinear Gas Spring Model Parameters

Variable	Parameter Name
x	Position
m	Mass
L	Gas Column Length
g	Gravity
A_p	Area of Diaphragm
P_3	Ambient Pressure
P_2	Cylinder Pressure
V_2	Cylinder Volume

The polytropic equation describes the pressure-volume relation:

$$P_2 = P_{20}\left(\frac{V_{20}}{V_2}\right)^n \tag{2.2}$$

with an initial volume of $V_{20} = A_p L$ and initial pressure P_{20}. The system is in equilibrium when

$$P_{20} = P_3 + mg/A_p \tag{2.3}$$

The volume as a function of displacement x is

$$V_2 = A_p(L - x) \tag{2.4}$$

Substituting Equations 2.2, 2.3, and 2.4 into Equation 2.1 yields

$$\begin{aligned}
\frac{\mathrm{d}^2x}{\mathrm{d}t^2} &= \frac{A_p}{m}\left[P_{20} - \frac{mg}{A_p} - P_{20}\left(\frac{A_p(L-x))}{A_pL}\right)^{-n}\right] + g \\
\frac{\mathrm{d}^2x}{\mathrm{d}t^2} &= \frac{A_pP_{20}}{m}\left[1 - \left(\frac{L-x}{L}\right)^{-n}\right] - \frac{mg}{A_p}\frac{A_p}{m} + g \\
\frac{\mathrm{d}^2x}{\mathrm{d}t^2} &= -\frac{A_pP_{20}}{m}\left[\left(1 - \frac{x}{L}\right)^{-n} - 1\right]
\end{aligned} \tag{2.5}$$

Andersen defines a linear pneumatic spring constant

$$k_p = \frac{nP_{20}(A_p)^2}{V_{20}} \tag{2.6}$$

Which can be rearranged and combined with the initial volume $V_{20} = A_p L$:

$$A_p P_{20} = \frac{k_p L}{n} \tag{2.7}$$

Substituting Equation 2.7 into Equation 2.5 yields

$$\frac{\mathrm{d}^2 x}{\mathrm{d}t^2} = -\frac{k_p L}{mn}\left[\left(1 - \frac{x}{L}\right)^{-n} - 1\right] \tag{2.8}$$

It is convenient to nondimensionalize the displacement using the length

$$\frac{\mathrm{d}^2\left(\frac{x}{L}\right)}{\mathrm{d}t^2} = -\frac{k_p}{mn}\left[\left(1 - \frac{x}{L}\right)^{-n} - 1\right] \tag{2.9}$$

Finally substitute $\eta = \frac{x}{L}$ for the per unit stroke and $\tau = \omega_n t$ where $\omega_n = \sqrt{\frac{k_p}{m}}$.

$$\frac{\mathrm{d}^2 \eta}{\mathrm{d}\tau^2} = -\frac{1}{n}\left[(1 - \eta)^{-n} - 1\right] \tag{2.10}$$

Figure 2.6 show the phase portrait of Equation 2.10 for a maximum initial velocity of 0.62. The phase portrait is a conveient way to display the response and mirrors that in the text to fit the convention used in the rest of this paper. Negative position is considered compression. The dashed vertical line represents the equilibrium position, to the left of the line, the system is being compressed; to the right of the line, the system is being extended. Note the two different curves shapes and that less displacement is required to stop the mass in compression compared to extension.

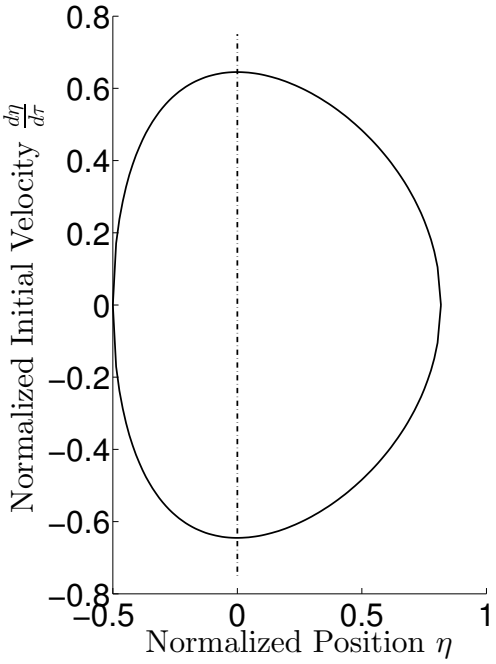

Figure 2.6: Analytical Phase Portrait Nonlinear Spring. Reproduced from [1]

2.2.5 Nondimensionalization of Damped Pneumatic Shock Isolators

Hundal has the most complete work on the analysis of pneumatic shock absorbers and vibration isolators [24–28]. These studies model the dynamics of damped pneumatic system with various configurations and base inputs. Although none pertain to the system under investigation here, they provide a guide for developing the nondimensional differential equations of motion and pressure.

2.2.6 Metal Bellows

One potential problem using long lengths of metal bellows under internal pressure is they can become unstable. Ooka et al. present an analysis showing how constrained metal bellows can

squirm under internal pressures [29]. Squirm is an instability similar to column buckling when a member is in compression. Due to this possibility, metal bellows manufactures configure metal bellows actuators such that the pressure is external to the bellows, eliminating the possibility of buckling in a similar way that a member in tension will not undergo Euler buckling [30, 31] .

2.2.7 Adaptive Pneumatic Impact Absorber

Mikułowski et al. have modeled and tested adaptive pneumatic impact absorbers [32, 33]. These devices consist of a piston with a piezoelectric valve built into the piston head that allows switching of the valve on the order of milliseconds. They did not offer any insight into how the analytical models were created. Instead, they showed the results of experiments and how well they matched with predictions. This research seems to be the most relevant and recent work on using pneumatics for impact absorption. It also shows the use of a fast switching valve as proposed in this research is practical.

CHAPTER 3: METHODOLOGY

Figure 3.1 shows the system under consideration. It consists of a mass on top of the metal bellows shock absorber. Control volume 2 (CV2) has a fixed volume while the volume of control volume 1 (CV1) is a function of bellows position. The top of the bellows is connected to the landing pad with a rod. The parameters are described in Table 3.1 and the nomenclature is similar to Hundal for easy cross reference.

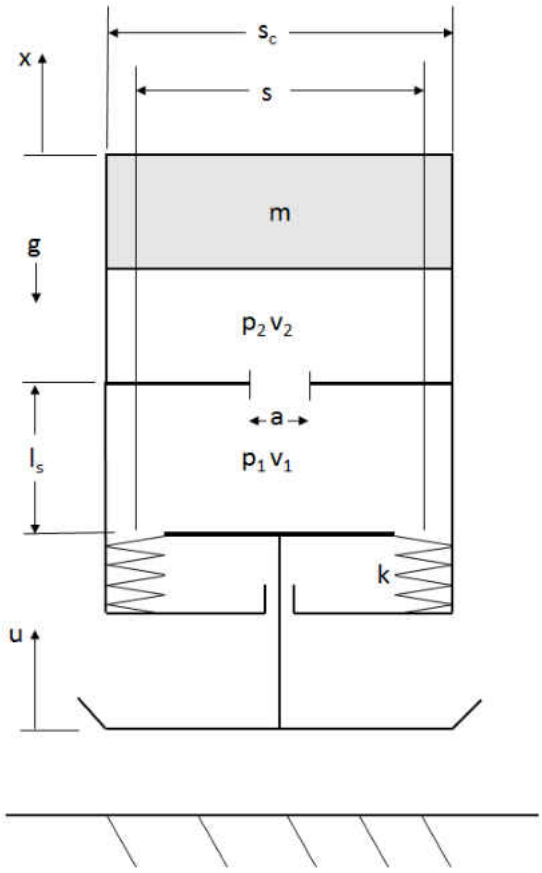

Figure 3.1: Pressurized Metal Bellows Shock Absorber

Table 3.1: Metal Bellows Shock Absorber Parameters

Variable	Parameter Name
x	Mass Position
u	Landing Pad Position
l_s	Bellows Stroke
s_c	Cylinder Area
s	Bellows Effective Area
p_i	control volume i Pressure
v_i	control volume i Volume
a	Orifice Area
m	Mass
g	Gravity
k	Bellows Spring Constant
R	Specific Gas Constant
n	Heat Capacity Ratio
C_0	Discharge Coefficient
θ	Temperature
Subscript	
$i, 1, 2$	control volume Number
u, d	upstream,downstream control volume
0	Initial Value
$'$	Time derivative

3.1 Metal Bellow Effective Area

Figure 3.2 shows a schematic of the Metal Bellows. To calculate the force on the bellows the effective area s of the bellows is required. The effective area is the area such that the force on the bellows will equal the pressure difference times this area, which is not the same as the outside dimension of the bellows.

Figure 3.2 is a typical diagram given by bellows manufacturers. Several manufacturers indicate that the effective area is based on the average of the inside radius r_i and outside radius r_o of the bellows [30, 31]. They use various justifications, such as pressure balance, but none are rigorous.

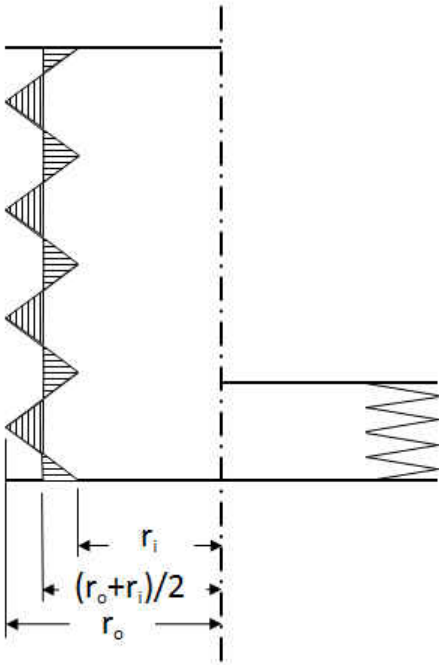

Figure 3.2: Metal Bellows Schematic

A better approach would be to calculate how the volume of the bellows changes with a change in length and use this change in volume to calculate pressure volume work. Figure 3.3 shows the dimensions for one diaphragm of an edge welded V shaped bellows. The volume of this section can be found from the volume integral. Note that this analysis is only valid for a bellows with diaphragms of this shape. There are many different diaphragm shapes and they would need to be treated independently.

The radius, corresponding area, and volume of the diaphragm cross section as a function of z are:

$$r = r_o \left(1 + \frac{z}{h}\left(\frac{r_i}{r_0} - 1\right)\right) \tag{3.1}$$

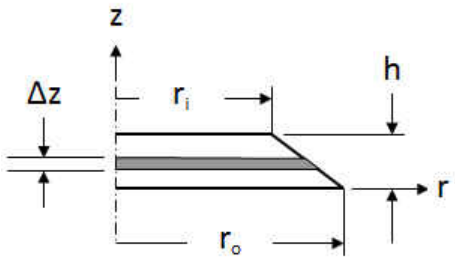

Figure 3.3: Volume of Diaphragm

$$A = \pi \left(r_o \left(1 + \frac{z}{h} \left(\frac{r_i}{r_0} - 1 \right) \right) \right)^2 \tag{3.2}$$

$$V = \int_0^h \pi r_o^2 \left(1 + \frac{z}{h} \left(\frac{r_i}{r_0} - 1 \right) \right)^2 dz$$

$$V = \frac{1}{3} \pi h \left(r_o^2 + r_o r_i + r_i^2 \right) \tag{3.3}$$

Equating pressure volume work with force acting through a change in height reveals an expression for the effective area.

$$PdV = Fdh$$

$$PdV = Psdh$$

$$s = \frac{\mathrm{d}V}{\mathrm{d}h} \tag{3.4}$$

$$s = \frac{\mathrm{d}V}{\mathrm{d}h} = \frac{1}{3} \pi \left(r_o^2 + r_o r_i + r_i^2 \right) \tag{3.5}$$

However, the manufacturers provide an effective area as

$$s = \pi \left(\frac{r_o + r_i}{2} \right)^2 = \frac{1}{4} \pi \left(r_o^2 + 2 r_0 r_i + r_i^2 \right) \tag{3.6}$$

These are clearly not equivalent. The results can be interpreted as the average of three terms r_o^2, $r_o r_i$, and r_i^2. The manufacturers' equation includes the $r_o r_i$ term twice. Letting $C = \frac{r_o}{r_i}$

$$\%\text{Error} = \frac{\frac{1}{3}\pi \left(C^2 + C + 1 \right) - \frac{1}{4}\pi \left(C^2 + 2C + 1 \right)}{\frac{1}{3}\pi \left(C^2 + C + 1 \right)} \tag{3.7}$$

Figure 3.4 shows the error as a function of C and asymptotes at 25% at extreme values of C. Table 3.2 shows values for ID and OD of bellows from a vendors catalog. The manufacturer's effective area and the effective area derived above are listed. The smallest bellows has an 8% error in the value. This analysis shows that care must be taken when calculating the effective area.

Table 3.2: Manufacturers' s vs Calculated s

r_o mm	r_i mm	Manufactures' s cm^2	Calculated s cm^2	% Difference
4.75	1.6	0.316	0.343	-8%
6.35	2.4	0.60	0.642	-7%
9.5	3.2	1.26	1.371	-8%
13.1	7.0	3.16	3.271	-3%
19.05	12.3	7.68	7.838	-2%
20.7	9.5	7.10	7.492	-5%
24	17.65	13.61	13.73	-1%

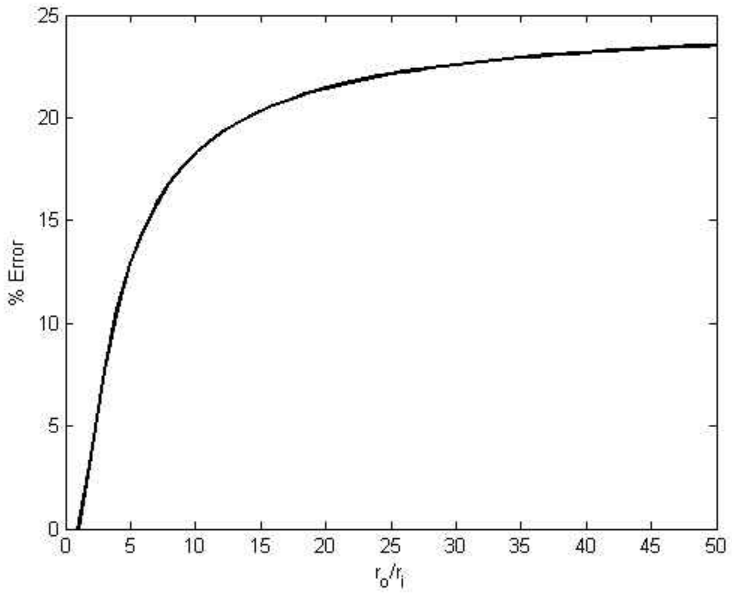

Figure 3.4: Volume Calculation Error

3.2 Metal Bellows Shock Absorber

The analysis on the dynamics of the metal bellows shock absorber follows the method used by Hundal [24, 27, 28]. The bellows actuator is shown in Figure 3.5a. After nondimensionalization, it is convenient to have an initial total volume of both control volumes equal to unity. The bellows is thus replaced with a piston with an area the same as the effective area of the bellows s and a spring with stiffness k as shown in Figure 3.5b.

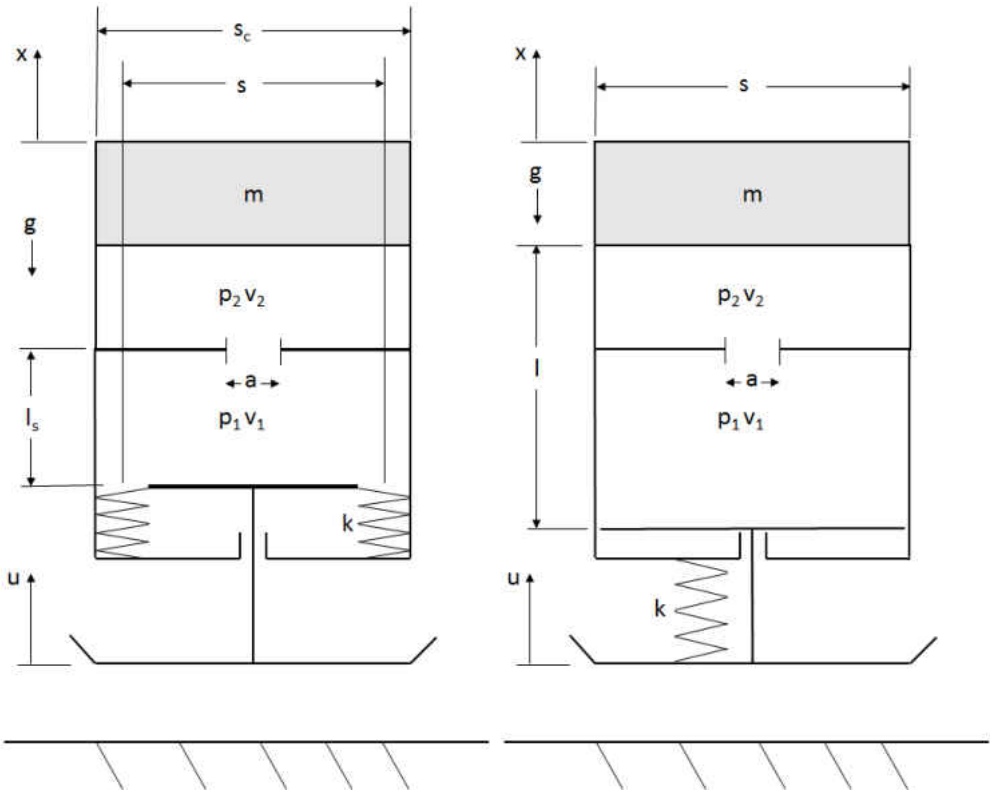

(a) Initial (b) Simplified

Figure 3.5: Metal Bellows Shock Absorber Schematic

It is assumed that there is little gas between the convolutions when the bellows is compressed. To

find the length l, we equate the volumes of the initial and simplified versions.

$$\begin{aligned} v_{\text{total initial}} &= v_{\text{total simplified}} \\ v_{10} + v_2 = s_c l_s + v_2 &= sl \\ l &= \frac{v_2 + s_c l_s}{s} \end{aligned} \tag{3.8}$$

However, this simplification creates a problem: in the initial schematic when the bellows reaches the physical end of stroke at $l_s = 0$, there will still be gas between the cylinder wall and bellows convolutions. In the simplified schematic the piston can displace all of the gas in CV1, which can never occur with the bellows. This will be addressed in Section 3.2.10.

3.2.1 Equation of Motion

The equation of motion for the mass position depends on whether the shock absorber landing pad is in contact with the surface.

$$mx'' = \begin{cases} -mg & \text{no surface contact} \\ p_1 s - kd - mg & \text{surface contact} \end{cases} \tag{3.9}$$

This piecewise function can alternately be expressed using the Heavyside function:

$$mx'' = \mathcal{H}\left(x \leq 0\right)\left(p_1 s - kd\right) - mg \tag{3.10}$$

Where $d = x - u$ is the relative displacement between the mass and the landing pad. In other words, the pressure and spring force of the bellows will only put a force on the mass when the foot is in contact with the ground.

Note that since the hopper is envisioned for small planetary bodies with no atmosphere, no external pressure is included. If there were an atmosphere, the force due to the pressure would need to be added to this equation. The sign of the kd term is also somewhat arbitrary. From communicating with a bellows manufacturers, the free length of the bellows can be set anywhere from compressed to extended [34]. In this analysis, it is assumed to be in the free state in the compressed configuration. During ground contact as x becomes negative and $u = 0$, d becomes negative and the $-kd$ term is positive, indicating an upward force on the mass. If the free state was changed so the free length was in the extended configuration the sign on the kd term would change to a positive.

3.2.2 Volume

The volumes of the control volumes are given as:

$$v_1 = v_{10} + sd \tag{3.11}$$

$$v_2 = sl - v_{10} \tag{3.12}$$

3.2.3 Ideal Gas Law

The gas is assumed to be ideal.

$$m_i = \frac{p_i v_i}{R\theta_i} \tag{3.13}$$

3.2.4 Adiabatic Compression

The process is assumed to be adiabatic which should hold if the compression is relatively quick.

$$\frac{\theta_i}{\theta_0} = \left(\frac{p_i}{p_0}\right)^{\frac{n-1}{n}}$$
$$\theta_i = \theta_0 p_i^{\frac{n-1}{n}} p_0^{\frac{1-n}{n}} \tag{3.14}$$

3.2.5 Conservation of mass

The conservation of mass between the two control volumes is

$$m_1' = -m_2' \tag{3.15}$$

3.2.6 Mass flow through an orifice

Mass flow of a compressible gas through an orifice is given by [35]

$$m_d' = \frac{C_0 a C_2 p_u}{\sqrt{R\theta_u}} \tag{3.16}$$

The mass flow depends upon the pressure ratios of the upstream to downstream pressure. Which side is considered upstream and downstream depends upon which pressure is higher. If this ratio is higher than a critical ratio, the flow velocity is sonic and the flow is choked. If it is less than the critical ratio the velocity is sub-sonic and the flow is non-choked. Determining if the flow is choked or non-choked is handled by the parameter C_2 as follows:

$$C_2 = \begin{cases} \sqrt{\frac{n}{\left(\frac{n+1}{2}\right)^{\frac{n+1}{n-1}}}} & \text{choked if } \frac{p_u}{p_d} > \left(\frac{n+1}{2}\right)^{\frac{n}{n-1}} \\ \left(\frac{p_d}{p_u}\right)^{\frac{1}{n}} \sqrt{\frac{2n}{n-1}\left(1-\frac{p_d}{p_u}\right)^{\frac{n-1}{n}}} & \text{non-choked if } \frac{p_u}{p_d} < \left(\frac{n+1}{2}\right)^{\frac{n}{n-1}} \end{cases}$$

The goal now is to derive equations for the mass flows for each control volume in terms of the initial values and instantaneous values of pressure. These equations will be used to derive the differential equations for pressure.

First, take the time derivatives of Equations 3.13, 3.14, 3.11, and 3.12.

$$m_i' = R^{-1}\theta_i^{-1}\left(p_i' v_i + p_i v_i' - p_i v_i \theta_i' \theta_i^{-1}\right) \tag{3.17}$$

$$\theta_i' = \theta_0 p_i' \left(\frac{n-1}{n}\right) {p_0}^{\frac{n-1}{n}} {p_i}^{\frac{-1}{n}} \tag{3.18}$$

$$v_1' = sd' \tag{3.19}$$

$$v_2' = 0 \tag{3.20}$$

Substitute Equations 3.14 and 3.18 into Equation 3.17.

$$\begin{aligned} m_i' &= R^{-1}\theta_0^{-1} {p_i}^{\frac{1-n}{n}} {p_0}^{\frac{n-1}{n}} \left(p_i' v_i + p_i v_i' - p_i v_i \theta_0 p_i' \left(\frac{n-1}{n}\right) {p_0}^{\frac{n-1}{n}} {p_i}^{\frac{-1}{n}} \theta_0^{-1} {p_0}^{\frac{n-1}{n}} {p_i}^{\frac{1-n}{n}}\right) \\ &= R^{-1}\theta_0^{-1} {p_i}^{\frac{1-n}{n}} {p_0}^{\frac{n-1}{n}} \left(p_i' v_i + p_i v_i' - v_i p_i' \left(\frac{n-1}{n}\right)\right) \\ &= R^{-1}\theta_0^{-1} {p_i}^{\frac{1-n}{n}} {p_0}^{\frac{n-1}{n}} \left(p_i v_i' + v_i p_i' n^{-1}\right) \\ &= R^{-1}\theta_0^{-1} {p_0}^{\frac{n-1}{n}} \left({p_i}^{\frac{1-n+n}{n}} v_i' + {p_i}^{\frac{1-n}{n}} v_i p_i' n^{-1}\right) \end{aligned}$$

$$m_i' = R^{-1}\theta_0^{-1}p_0^{\frac{n-1}{n}}n^{-1}p_i^{\frac{1}{n}}\left(nv_i' + v_i p_i' p_i^{-1}\right) \tag{3.21}$$

For i=1 and substituting in Equation 3.11 and 3.19

$$m_1' = R^{-1}\theta_0^{-1}p_0^{\frac{n-1}{n}}n^{-1}p_1^{\frac{1}{n}}\left(nsd' + (v_{10} + sd)\, p_1' p_1^{-1}\right) \tag{3.22}$$

For i=2 and substituting in Equation 3.12 and 3.20

$$m_2' = R^{-1}\theta_0^{-1}p_0^{\frac{n-1}{n}}n^{-1}v_2 p_2' p_2^{\frac{1-n}{n}} \tag{3.23}$$

3.2.7 Nondimensional Parameters

Before going forward with further simplification the equations will be cast in nondimensional form using the following definitions where x_0' and p_0 are arbitrary scaling factors that can be chosen for convenience.

Displacements

$$X = \frac{x}{l} \qquad U = \frac{u}{l} \qquad D = \frac{d}{l}$$

Velocities

$$\dot{X} = \frac{x'}{x'_0} \qquad \dot{U} = \frac{u'}{x'_0} \qquad \dot{D} = \frac{d'}{x'_0}$$

Accelerations

$$\ddot{X} = \frac{x''l}{x'^2_0} \qquad \ddot{U} = \frac{u''l}{x'^2_0} \qquad \ddot{D} = \frac{d''l}{x'^2_0}$$

Volumes

$$V_{10} = \frac{v_{10}}{sl} \qquad V_2 = \frac{v_2}{sl} = 1 - V_{10}$$

Pressures

$$P_i = \frac{p_i}{p_0} \qquad \dot{P}_i = \frac{\dot{p}_i l}{p_0 x'_0}$$

Time	Gravity	Bellows Ratio
$T = \frac{t x'_0}{l}$	$G = \frac{gl}{x'^2_0}$	$B = \frac{s}{s_c}$
Mass	**Stiffness**	**Area Ratio**
$M = \frac{m x'^2_0}{p_0 s l}$	$K = \frac{kl}{p_0 s}$	$S = \frac{naC_0\sqrt{R\theta_0}}{s x'_0}$

3.2.8 Nondimensional Equation of Motion

For the nondimensional equation of motion of the position of the mass, begin with Equation 3.10, substitute in nondimensional terms, and simplify:

$$Mp_0 slx_0'^{-2} X'' x_0'^2 l^{-1} = \mathcal{H}\left(Xl \leq 0\right)\left(P_1 p_0 s - K p_0 s l^{-1} D l\right) - Mp_0 slx_0'^{-2} G x_0'^2 l^{-1}$$

$$MX'' = \mathcal{H}\left(X \leq 0\right)\left(P_1 - KD\right) - MG \tag{3.24}$$

3.2.9 Nondimensional Mass Flow

For the nondimensional equations for mass flow, begin with Equation 3.22, 3.23, 3.16 and 3.15, substitute in nondimensional terms, and simplify:

$$\begin{aligned}
m_1' &= R^{-1}\theta_0^{-1} p_0^{\frac{n-1}{n}} n^{-1} p_0^{\frac{1}{n}} P_1^{\frac{1}{n}} \left(ns\dot{D}x_0' + \left(V_{10}sl + sDl\right) p_0 v_e l^{-1} \dot{P}_1 p_0^{-1} P_1^{-1}\right) \\
&= R^{-1}\theta_0^{-1} s x_0' p_0 n^{-1} P_1^{\frac{1}{n}} \left(n\dot{D} + \left(V_{10} + D\right)\dot{P}_1 P_1^{-1}\right) \\
m_1' &= aC_0 p_0 S^{-1} R^{\frac{-1}{2}} \theta_0^{\frac{-1}{2}} P_1^{\frac{1-n}{n}} \left(n\dot{D}P_1 + \left(V_{10} + D\right)\dot{P}_1\right) \qquad (3.25) \\
m_2' &= R^{-1}\theta_0^{-1} p_0^{\frac{n-1}{n}} n^{-1} V_2 sl\dot{P}_2 p_0 x_0' l^{-1} P_2^{\frac{1-n}{n}} p_0^{\frac{1-n}{n}} \\
&= R^{-1}\theta_0^{-1} p_0 n^{-1} V_2 s\dot{P}_2 x_0' P_2^{\frac{1-n}{n}} \\
m_2' &= aC_0 p_0 S^{-1} R^{\frac{-1}{2}} \theta_0^{\frac{-1}{2}} \dot{P}_2 P_2^{\frac{1-n}{n}} V_2 \qquad (3.26) \\
m_d' &= aC_0 C_2 R^{\frac{-1}{2}} P_u p_0 \left(\theta_0 p_0^{\frac{1-n}{n}} p_u^{\frac{n-1}{n}}\right)^{\frac{-1}{2}} \\
&= aC_0 C_2 R^{\frac{-1}{2}} \theta_0^{\frac{-1}{2}} P_u p_0 p_0^{\frac{n-1}{2n}} p_0^{\frac{1-n}{2n}} P_u^{\frac{1-n}{2n}} \\
m_d' &= aC_0 C_2 R^{\frac{-1}{2}} \theta_0^{\frac{-1}{2}} p_0 P_u^{\frac{1+n}{2n}} \qquad (3.27) \\
m_u' &= -aC_0 C_2 R^{\frac{-1}{2}} \theta_0^{\frac{-1}{2}} p_0 P_u^{\frac{1+n}{2n}} \qquad (3.28)
\end{aligned}$$

Now nondimensional equations for mass flow for CV1 and 2 have been derived from the time derivatives of the Ideal Gas Law, Adiabatic Compression, and Volume equations. In addition, a nondimensional equation represents the mass flow through an orifice. The next step is setting the

mass flow equations from the time derivatives and from the flow through an orifice equal to each other based on gas flow direction. There are two cases to consider for the flow between control volumes. Consider first $P_1 > P_2$. In this case, gas will flow from CV1 to CV2, so $P_u = P_1$ and $P_d = P_2$ (with $u = 1$ and $d = 2$).

Equating the two expressions for mass flow in CV1 (Equations 3.25 and 3.28) yields:

$$\begin{aligned} m_1' &= m_1' \\ aC_0p_0S^{-1}R^{\frac{-1}{2}}\theta_0^{\frac{-1}{2}}P_1^{\frac{1-n}{n}}\left(n\dot{D}P_1 + (V_{10}+D)\dot{P}_1\right) &= -aC_0C_2R^{\frac{-1}{2}}\theta_0^{\frac{-1}{2}}p_0P_1^{\frac{1+n}{2n}} \\ n\dot{D}P_1 + (V_{10}+D)\dot{P}_1 &= -C_2SP_1^{\frac{1+n}{2n}}P_1^{\frac{n-1}{n}} \\ n\dot{D}P_1 + (V_{10}+D)\dot{P}_1 &= -C_2SP_1^{\frac{3n-1}{2n}} \end{aligned} \tag{3.29}$$

Similarly for the mass flow in CV2 (Equations 3.26 and 3.27) yields:

$$\begin{aligned} m_2' &= m_2' \\ aC_0p_0S^{-1}R^{\frac{-1}{2}}\theta_0^{\frac{-1}{2}}\dot{P}_2P_2^{\frac{1-n}{n}}V_2 &= aC_0C_2R^{\frac{-1}{2}}\theta_0^{\frac{-1}{2}}p_0P_1^{\frac{1+n}{2n}} \\ S^{-1}\dot{P}_2P_2^{\frac{1-n}{n}}V_2 &= C_2P_1^{\frac{1+n}{2n}} \\ \dot{P}_2V_2 &= C_2SP_1^{\frac{1+n}{2n}}P_2^{\frac{n-1}{n}} \end{aligned} \tag{3.30}$$

Consider now the case $P_1 < P_2$. In this case gas, will flow from CV2 to CV1 so $P_u = P_2$ and $P_d = P_1$ (with $u = 2$ and $d = 1$). Again begin by equating the two expressions for mass flow in CV2 (Equations 3.25 and 3.27) yields:

$$\begin{aligned} m_1' &= m_1' \\ aC_0p_0S^{-1}R^{\frac{-1}{2}}\theta_0^{\frac{-1}{2}}P_1^{\frac{1-n}{n}}\left(n\dot{D}P_1 + (V_{10}+D)\dot{P}_1\right) &= aC_0C_2R^{\frac{-1}{2}}\theta_0^{\frac{-1}{2}}p_0P_2^{\frac{1+n}{2n}} \\ S^{-1}P_1^{\frac{1-n}{n}}\left(n\dot{D}P_1 + (V_{10}+D)\dot{P}_1\right) &= C_2P_2^{\frac{1+n}{2n}} \end{aligned}$$

$$n\dot{D}P_1 + (V_{10} + D)\,\dot{P}_1 = SC_2 P_1^{\frac{n-1}{n}} P_2^{\frac{1+n}{2n}} \tag{3.31}$$

Similarly for the mass flow in CV2 (Equations 3.26 and 3.28) yields:

$$\begin{aligned}
m_2' &= m_2' \\
aC_0 p_0 S^{-1} R^{\frac{-1}{2}} \theta_0^{\frac{-1}{2}} \dot{P}_2 P_2^{\frac{1-n}{n}} V_2 &= -aC_0 C_2 R^{\frac{-1}{2}} \theta_0^{\frac{-1}{2}} p_0 P_2^{\frac{1+n}{2n}} \\
S^{-1} \dot{P}_2 P_2^{\frac{1-n}{n}} V_2 &= -C_2 P_2^{\frac{1+n}{2n}} \\
\dot{P}_2 V_2 &= -C_2 S P_2^{\frac{1+n}{2n}} P_2^{\frac{n-1}{n}} \\
\dot{P}_2 V_2 &= -C_2 S P_2^{\frac{1+n+2n-2}{2n}} \\
\dot{P}_2 V_2 &= -C_2 S P_2^{\frac{3n-1}{2n}}
\end{aligned} \tag{3.32}$$

In summary, equations 3.24, 3.29, 3.30, 3.31, and 3.32 are the nondimensional differential equations for this system.

3.2.10 Boundary Conditions

For the numerical analysis of this problem, the base motion needs to be constrained. When the system is not in contact with the surface, the relative velocity $\dot{D} = 0$. When the system is in contact with the ground the velocity $\dot{U} = 0$. When the system reaches the stroke limit the top of the bellows will impact the housing and the device will "bottom out" as shown in Figure 3.6. To determine when the shock absorber will bottom out the minimum value of D needs to be determined.

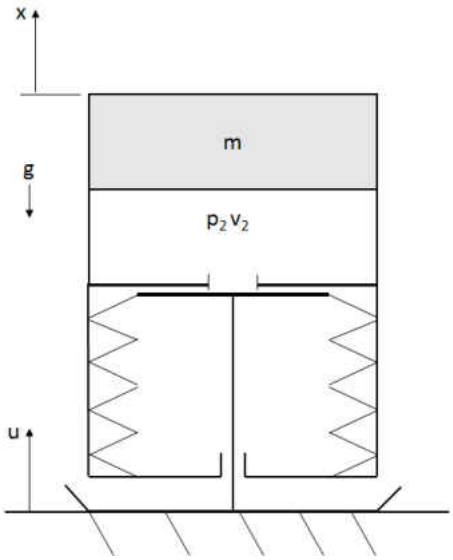

Figure 3.6: Metal Bellows Shock Absorber Bottoming Out

Referring to Figure 3.1, the bellows will bottom out when $d < -l_s$. In nondimensional terms, this inequality is

$$\begin{aligned} D &< -\frac{l_s}{l} \\ &< -\frac{sl_s}{v_2 + s_c l_s} \\ &< -\frac{Bs_c l_s}{v_2 + s_c l_s} \\ &< -\frac{Bv_{10}}{v_2 + v_{10}} \\ &< -\frac{BV_{10}}{V_2 + V_{10}} \\ D &< -BV_{10} \end{aligned} \tag{3.33}$$

From this point on the terms bottoming out and stroke limit will refer to the situation described in Equation 3.33. Therefore, when $D < -BV_{10}$, a spring of stiffness K_b will come into effect to simulate an impact of the bellows bottoming out. Adding this spring to the equation of motion 3.24 yields:

$$MX'' = \mathcal{H}\left(X \leq 0\right)\left(P_1 - KD\right) - \mathcal{H}\left(D < -BV_{10}\right)K_b\left(BV_{10} + D\right) - MG \tag{3.34}$$

3.3 Initial Design Equations

The differential equations are nonlinear, and in general need to be solved numerically to determine the response. Estimating or providing bounds to the response before running the numerical analysis can help determine parameters to make the numerical analysis more efficient and stable. These equations are also required to select paramter values when implementing an active control system.

3.3.1 Static Equilibrium Solution

The static equilibrium solution is of interest to determine at what position the system will eventually come to rest. Starting with Equation 3.34, sum the forces acting on the mass and require them to balance.

$$0 = P_1 - KD - MG \tag{3.35}$$

Note that P_1 is a function of D. At steady state the pressure in both control volumes will be equal. Using the polytropic Equation 2.2 for the total volume of both control volumes

$$P_1 = P_0\left(\frac{sl}{s\left(l + d\right)}\right)^n = P_0\left(\frac{1}{\left(1 + D\right)}\right)^n \tag{3.36}$$

Substituting Equation 3.36 into Equation 3.35, the balance of forces is now

$$0 = P_0 \left(\frac{1}{(1+D)} \right)^n - KD - MG \tag{3.37}$$

Equation 3.37 can be solved for D using a nonlinear solver such as MATLAB's fzero. One interesting case can be solved analytically. If it is assumed $P_0 = K = MG$ then Equation 3.37 simplifies to

$$0 = \left(\frac{1}{(1+D)} \right)^n - D - 1$$

or

$$D + 1 = \left(\frac{1}{(1+D)} \right)^n \tag{3.38}$$

For this special case, the equation only holds for $D = 0$, which provides a convenient check for the numerical analysis. The static equilibrium equation provides a tool for the selection of parameters. If there is a desired value of D for the static equilibrium (e.g., coming to rest bottomed out) then $D = -BV_{10}$ can be substituted into Equation 3.37, which provides a constraint on the other parameters. Since most likely M and G will be given, P_0 and K can be calculated for the desired value of D.

3.3.2 Maximum Initial Displacement Bounds

The maximum initial displacement of the system, where $\dot{D} = 0$ on the first cycle, is nonlinear with no general analytical solution. However, the bounds can be found for two special cases, the upper bound, when the orifice is closed ($a = 0$), and the lower bound, when the orifice is the same as the effective area ($a = s$). The upper bound and only considers CV1 and will result in a smaller displacement. The lower bound considers both control volumes and will result in a larger

displacement. The real stroke will be between these upper and lower bounds and depends on the value of S.

To find these bounds work/energy is used. The change in kinetic energy, gravitational potential energy, and spring potential energy from the initial conditions to the displacement that brings the system to rest is set equal to the work required to compress the gas. First, the equations for energy and work are derived and nondimensionalized. Change in kinetic energy from x_0' to 0

$$\Delta KE = \frac{1}{2} m x_0'^2 = \frac{1}{2} \frac{M p_0 s l}{x_0'^2} \left(\dot{X}_0 x_0' \right)^2$$
$$\Delta KE = (p_0 s l) \frac{1}{2} M \dot{X}_0^{\,2} \tag{3.39}$$

Change in potential energy from gravity

$$\Delta PE_g = mg\Delta h = mg\,(x_0 - d) = \frac{M p_0 s l}{x_0'^2} \frac{G x_0'^2}{l} \left(X_0 l - D l \right)$$
$$\Delta PE_g = (p_0 s l)\, MG\,(X_0 - D) \tag{3.40}$$

The work compressing the gas from the initial volume (v_0) to the final volume (v_f) is

$$W_c = \int_{v_0}^{v_f} p dv$$

Using polytropic compression Equation 2.2, substituting in nondimensional terms, and simplifying yields:

$$p = p_{10} v_0^n v^{-n}$$
$$W_c = \int_{v_0}^{vf} p_{10} v_0^n v^{-n} dv$$
$$= \frac{p_{10} v_0^n v^{1-n}}{1-n} \Bigg|_{v_0}^{vf}$$

$$
\begin{aligned}
&= \frac{p_{10} v_0^n}{1-n} \left(v_f^{1-n} - v_0^{1-n} \right) \\
&= \frac{P_{10} p_0 \left(V_0 sl \right)^n}{1-n} \left(\left(V_f sl \right)^{1-n} - \left(V_0 sl \right)^{1-n} \right) \\
&= \frac{P_{10} p_0 V_0^n \left(sl \right)^n \left(sl \right)^{1-n}}{1-n} \left(V_f^{1-n} - V_0^{1-n} \right) \\
W_c &= \left(p_0 sl \right) \frac{P_{10} V_0^n}{1-n} \left(V_f^{1-n} - V_0^{1-n} \right)
\end{aligned}
\tag{3.41}
$$

Next, the nondimensional volumes for two cases are determined. When the orifice is closed the initial volume is the volume of CV1 and when the orifice is fully opened the initial volume is the volume of both control volumes. The final volume is the initial volumes plus the displacement D. This can be written as

$$
\begin{aligned}
V_0 &= \begin{cases} V_{10} & \text{if } a = 0 \\ 1 & \text{if } a = s \end{cases} \\
V_f &= \begin{cases} V_{10} + D & \text{if } a = 0 \\ 1 + D & \text{if } a = s \end{cases}
\end{aligned}
\tag{3.42}
$$

Substituting Equation 3.42 into Equation 3.41 yields:

$$
W_c = \left(p_0 sl \right) \frac{P_{10}}{1-n} \begin{cases} \left(\left(1 + D \right)^{1-n} - 1 \right) & \text{if } a = 0 \\ V_{10}^n \left(\left(V_{10} + D \right)^{1-n} - V_{10}^{1-n} \right) & \text{if } a = s \end{cases}
\tag{3.43}
$$

Next, consider the change in the energy stored in the bellows spring. In this case, the free length is

when the bellows is fully compressed.

$$\Delta PE_{sp} = \frac{1}{2}k\Delta d^2 = \frac{Kp_{10}s}{2l}D^2l^2$$
$$\Delta PE_{sp} = (p_{10}sl)\,\frac{1}{2}KD^2 \tag{3.44}$$

Finally, the nonlinear static equilibrium equation in terms of D can be established. Note each term has a $p_{10}sl$ term that can be eliminated from the equation leaving it nondimensional. The term for potential energy in the spring is negative because as the shock absorber displacement increases energy is stored in the spring. Equation 3.45 can be solved for D using numerical methods.

$$\Delta KE + \Delta PE_g(D) - \Delta PE_{sp}(D) + W_c(D) = 0 \tag{3.45}$$

3.3.3 Estimated Natural Frequency

The numerical integration of the nonlinear differential equations needs to occur over a finite time. If this time is too long and includes when the system has a small response, numerical errors will start accumulating and the time to run the analysis will increase. It is therefore preferable to integrate for a certain number of cycles; to do so, however requires an estimate of the natural frequency. Start with the equation for natural frequency of a spring mass system, substitute in the linear pneumatic spring constant given by Equation 2.6, substitute in nondimensional terms, and simplify.

$$f_n = \sqrt{\frac{k}{m}}$$
$$\frac{1}{t} = \frac{1}{2\pi}\sqrt{\frac{k_p + k}{m}}$$

$$
\begin{aligned}
\frac{1}{t} &= \frac{1}{2\pi}\sqrt{\left(\frac{np_{10}s^2}{v_{10}} + k\right)\frac{1}{m}} \\
\frac{x_0'}{Tl} &= \frac{1}{2\pi}\sqrt{\left(\frac{nP_{10}p_0s^2}{V_{10}sl} + \frac{Kp_0s}{l}\right)\frac{x_0'^2}{Mp_0sl}} \\
\frac{x_0'}{Tl} &= \frac{1}{2\pi}\sqrt{\left(\frac{nP_{10}}{V_{10}} + K\right)\frac{1}{M}\frac{x_0'^2}{l^2}} \\
\frac{1}{T} &= \frac{1}{2\pi}\sqrt{\left(\frac{nP_{10}}{V_{10}} + K\right)\frac{1}{M}}
\end{aligned}
\tag{3.46}
$$

3.4 Control Concepts

Passive damping may be sufficient for some applications; however, several control concepts can provide additional performance benefits and prompt an interesting analysis.

3.4.1 Check Valve and Orifice Concept

The first control system is to add a check valve of area a_c between the control volumes as shown in Figure 3.7. The idea is that restricting the flow during expansion will reduce the bounce by lowering the pressure in CV1. The fixed orifice will allow the pressure to eventually stabilize between the control volumes, allowing the system to return to static equilibrium. To model the check valve, a non-dimensional parameter C is introduced as the ratio of the orifice area when $P_2 > P_1$ to the total orifice area when $P_1 > P_2$:

$$
C = \frac{a}{a_c + a} \tag{3.47}
$$

The default case of the same orifice area in both directions is when $C = 1$ and when $C = 0$ the return orifice would be closed off and gas can only flow in one direction.

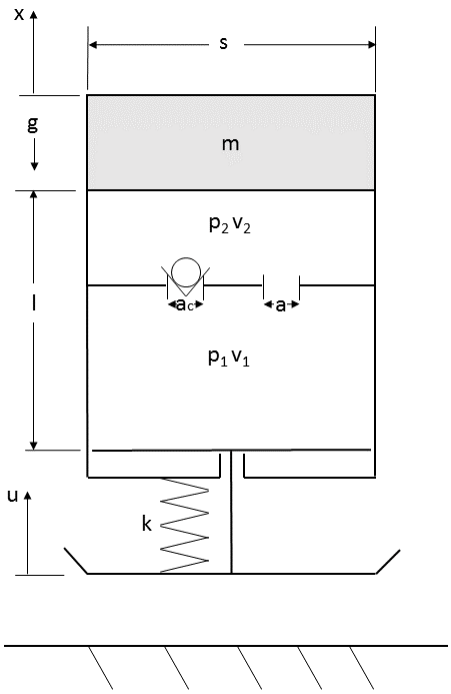

Figure 3.7: Bellows Actuator Schematic with Check Valve and Orifice

The control concept can be implemented in the equations of motion by modifying the area ratio S as follows:

$$S = \begin{cases} S & \text{if } P_1 > P_2 \\ CS & \text{if } P_1 < P_2 \end{cases}$$

3.4.2 *On/Off Valve Control Concept*

Another control concept replaces the orifice with an active valve, as depicted in Figure 3.8. The valve would be opened and closed to achieve maximum damping and minimize bounce. This control concept only operates twice during the compression stroke and so would require minimum power; furthermore, it only requires the initial impact velocity as an input.

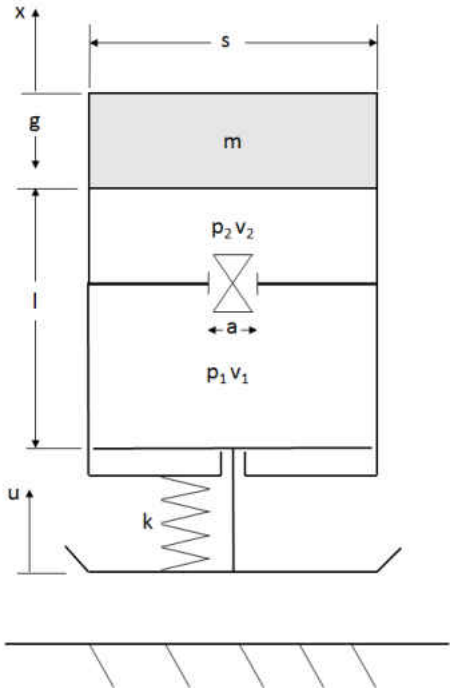

Figure 3.8: Bellows Actuator Schematic with Active Valve

The system will oscillate around static equilibrium with the valve open. System parameters need to be chosen so the upper bound is above the static equilibrium which is above the bottom. If the upper bound is below the static equilibrium, even if the valve is left closed, the shock absorber will not stop before static equilibrium is reached and no control is possible.

With the parameters selected, the timing of the valve needs to be found for each initial velocity. The valve will initially be open and then closed at some time T_1 such that the upper bound will equal the static equilibrium position. Then near the static equilibrium position the valve will be opened at T_2, equalizing the pressure in the control volumes and bringing the system to rest.

3.4.3 Adaptive Control Concept

A final control concept opens and closes the valve multiple times during the compression stroke to achieve the goal of bringing the system to rest at the static equilibrium. This control concept requires instantaneous displacement, velocity, and acceleration as an input and, since the valve is continuously operating, would require a more powerful and faster acting valve than the on/off concept.

The control scheme is to take the current position and velocity of the system and calculate the acceleration required to bring the system to rest at the static equilibrium along a predetermined profile. This acceleration is compared to the actual acceleration and the valve is opened and closed to try to maintain the correct acceleration.

The profile chosen here is the exponential decay such that the position, velocity, and acceleration all end up at zero at the same time.

$$\begin{aligned} X &= Ae^{-\zeta t} \\ \dot{X} &= -A\zeta e^{-\zeta t} \\ \ddot{X} &= A\zeta^2 e^{-\zeta t} \end{aligned} \tag{3.48}$$

At each point in time during the compression stroke $t = 0$ the coefficient A and ζ are calculated using the current distance from static equilibrium X_c and velocity $\dot{X}_c$ ($A = X_c$ and $\zeta = -\dot{X}_c/X_c$). These values are then substituted into the acceleration equation and compared to the current acceleration to determine if the valve should be opened or closed.

$$\begin{aligned} \ddot{X} &= A\zeta^2 \\ \ddot{X} &= X_c \left(\frac{\dot{X}_c}{-X_c} \right)^2 \\ \ddot{X} &= \frac{\dot{X}_c^{\,2}}{X_c} \end{aligned} \tag{3.49}$$

3.4.4 On/Off Valve Hopping

Another use for an on/off valve is for initiating a hop. This technique can be simulated using the equations of motion developed, though with different initial conditions. In general, the numerical analyses start at $X = 0$, $\dot{X} = -1$, and $P_{10} = P_{20}$, which is the device just in contact with the surface with some downward velocity and the pressure in both control volumes identical. To initiate a hop, the initial conditions will start with the device at static equilibrium with zero velocity and the pressure in P_1 in static equilibrium and P_2 higher.

It should be noted that actual maximum height reached during launch is based, in this model, on uniform gravity. If this technique were used on a very low gravity body where the gravitational force changed significantly during the hop, the constant gravity model would need to be replaced with the actual gravitational field. The more accurate value in this analysis would be the velocity as the system leaves the surface which could then be used at the initial value for the orbital mechanics analysis.

3.5 Optimization

If passive shock absorbers are used it is important to select the parameter values, that the designer has control over, to achieve the design goals and maximize performance. Most likely, things like gravity, mass, and maximum initial velocity will be given. The designer will have control over pressure, stroke, areas, and bellows stiffness. A method to optimize these parameter values will be developed.

3.5.1 Nondimensional Optimization

In order to optimize the design parameters in nondimensional terms, an objective function and criteria are defined and shown in Table 3.3. The objective function is to maximize the damping coefficient ζ, and the criteria are that the system will not rebound off the surface and the shock absorber will not bottom out.

Table 3.3: Optimization Criteria

Criteria	Condition
Maximize Damping	$\max(\zeta)$
No Rebound	$\max(X) \leq 0$
No Bottoming Out	$\min(X) > -BV_{10}$

The objective function will be used to rank the results. Since this system is nonlinear, picking the peaks and fitting an exponential curve using a linear regression does not work well. The initial response is very nonlinear and then decays, oscillating around the static equilibrium at a constant amplitude. Therefore, the proposed damping model is used.

$$X = A \sin \omega t \left(e^{-\zeta t} + B \right)$$

Trying to directly fit this equation to the peaks is problematic because the first few peaks tend to be very nonlinear and result in a poor fit. To help compensate for this, the absolute value of the distance between the position and static equilibrium value is integrated. Then using MATLAB's nonlinear fit function fitln the coefficients of the equation are determined. Figure 3.9 shows this process with an example viscous damping response. First, the absolute value of the response is plotted. Then the equation is integrated and plotted. MATLAB fitln is called on this numerical data with the model given above. Then the models are plotted with the coefficients from the fit which show a good correlation.

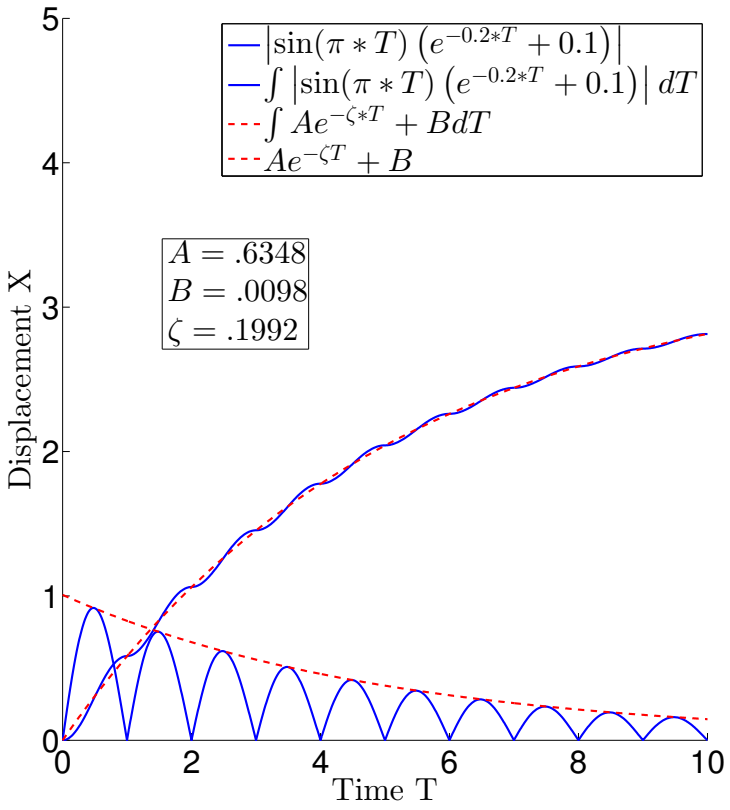

Figure 3.9: Illustration of Damping Model Methodology

3.5.2 Dimensional Optimization Using Vendors Data

This analysis will be similar to the nondimensional optimization except that given dimensional parameter values will be used. The goal will be to find a solution that meets the criteria, and the objective function will be the lowest mass system. Vendors give information on the bellows in terms of one capsule and actual values depend on the number of capsules selected. In this optimization the program will loop for each size capsule, through the number of capsules, until an acceptable solution is reached. In order to speed up the calculations, before the numerical integration, a check of the upper bound is made. If the upper bound is greater than the available

stroke the program is looped without running the numerical integration. Also, because the natural frequencies of this system vary considerably with the parameters, the numerical integration is run for two cycles at first, which allows the criteria to be checked. If the criteria are fulfilled, the numerical integration is run for ten cycles and the response will be used to determine the damping coefficient. Then the mass for each solution will be compared and the one with the lowest mass will be selected.

CHAPTER 4: FINDINGS

The objective of this chapter is to try to verify the models created in the previous chapter. No physical experiments were conducted in this research. Verification will consists of comparing the results with previous work, varying the parameters to see if the response changes in a logical way, and determining if the numerical simulations agree with the analytical results for special cases.

4.1 Initial Verification

To verify the code and dynamics model, the first run was taken with initial conditions similar to the case in Andersen nonlinear pneumatic spring analysis. The equations of motion integrated numerically. The initial conditions were $X_0 = 0$ and $\dot{X} = 0$ An initial volume $V_{10} = 1$ ensured the system did not bottom out. The orifice was closed so there would be no damping $S = 0$. The results are plotted in a phase portrait in Figure 4.1. The minimum displacement was used for the Andersen solution and this was plotted as well. The difference between the two plots in the velocity axis is due to the difference in the nondimensional time terms. Andersen scales time with the natural frequency and this analysis uses the initial impact velocity. Anderson's solution also has an external pressure which is why the maximum displacement is lower than for this analysis. Even with these differences the general shape of being a larger radius curve in compression than in extension is evident.

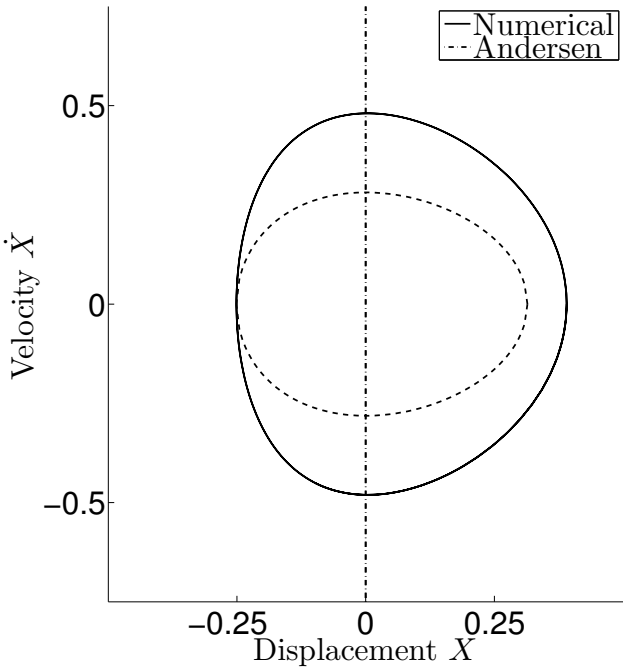

Figure 4.1: Non Damped Phase Diagram

To show the effect of varying each parameter value, plots of displacement, acceleration and phase portrait are shown for nominal values shown in Table 4.1. The response is shown in Figure 4.2. The initial displacement is when the base just contacts the ground and there is an initial downward velocity $X_0 = 0, \dot{X}_0 = -1$. Negative displacements correspond to compression of the device; positive displacements correspond to the hopper above the surface (not in contact). The hopper leaving the surface can be seen where the acceleration jumps to a constant value of $G = -1$. That is, the hopper is not in contact with the surface when $X > 0$, so the only applied force is due to gravity. These parameter values are the ones discussed in the static equilibrium solution section that resulted in a static equilibrium value of $D = 0$. The phase portrait shows a decreasing spiral towards equilibrium, which gives a qualitative way of comparing damping ratios. The faster the spiral approaches equilibrium the higher the damping ratio. Finally, the point where the shock

absorber bottoms out for the default case will be $BV_{10} = 0.5$.

Table 4.1: Nominal Parameter Values

Parameter	n	M	S	B	V_{10}	G	K	X_0	$\dot{X}_0$	P_0
Value	1.4	1	.5	1	.5	1	1	0	-1	1

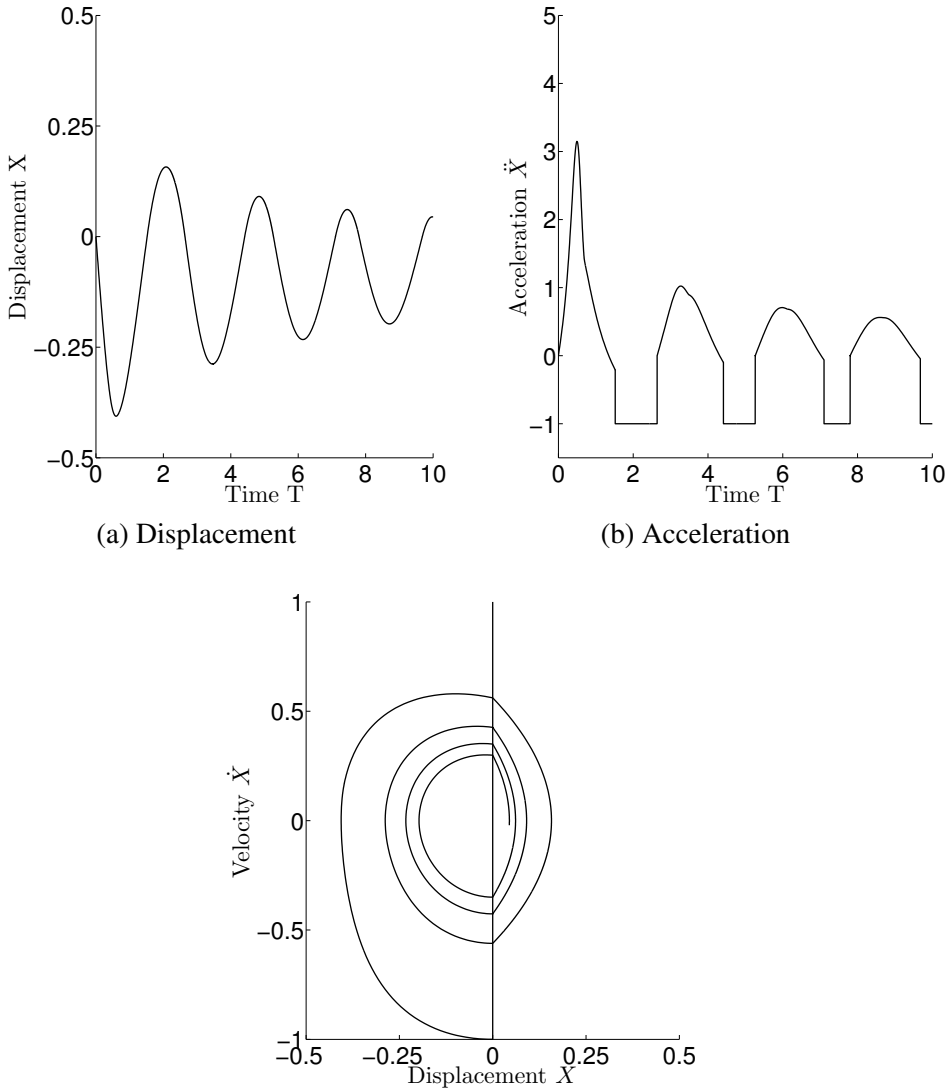

(a) Displacement

(b) Acceleration

(c) Phase Portrait

Figure 4.2: Response for Nominal Values

Next, one by one each parameter value is varied while the others are left at their nominal values, to demonstrate how the parameters effect system response around this particular point. The nominal response will be in a black solid line while the varied parameter will be in color: blue or green if the parameter is less than its nominal value and red or purple if greater than its nominal value.

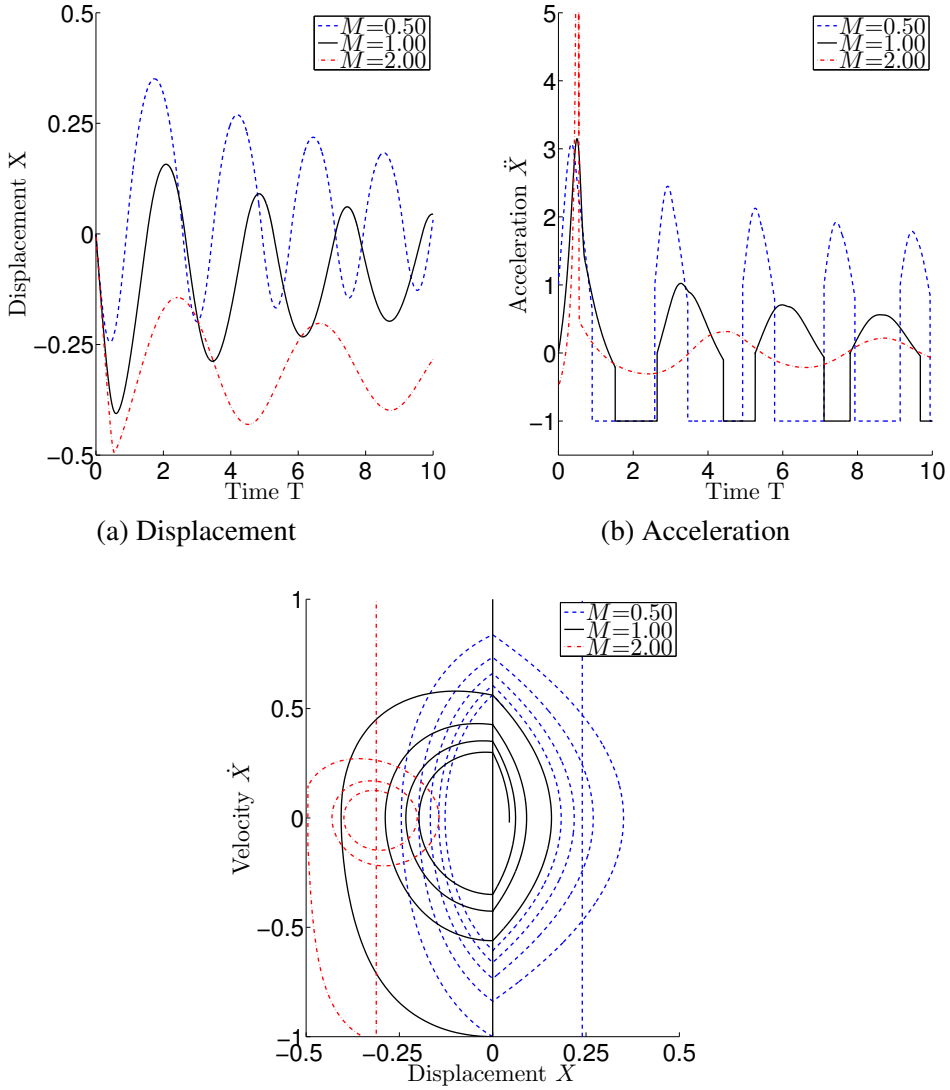

(a) Displacement

(b) Acceleration

(c) Phase Portrait

Figure 4.3: Varying Mass M

Figure 4.3 shows an increasing mass has a larger displacement in the first cycle. In addition, each response oscillates around its own static equilibrium value, which decreases as the mass is increased. This conforms with intuition that a larger mass will compress the shock absorber more. The response for $M = 2$ is very close to bottoming out which will happen at $X = -0.5$. The results show a very sharp response in displacement and a peak in acceleration. For $M = 2$ the device never leaves the ground and in the phase portrait heads towards equilibrium the quickest.

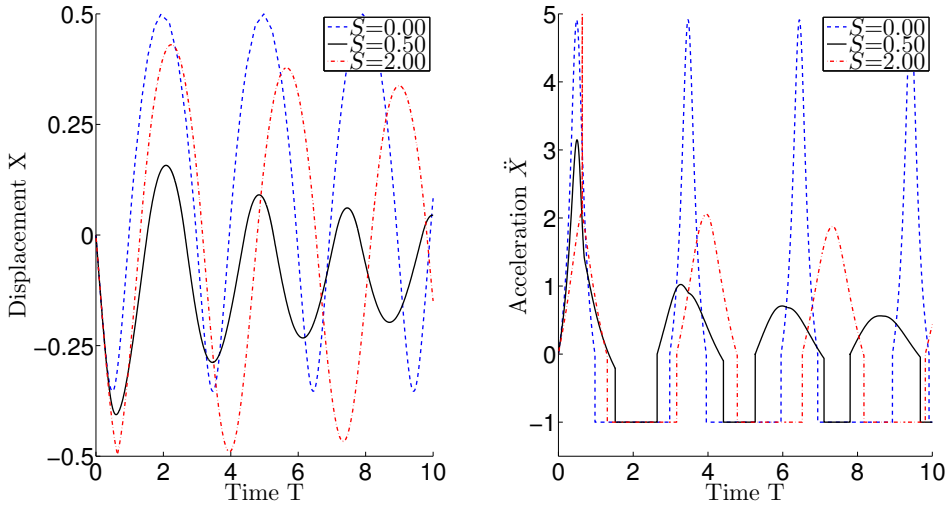

(a) Displacement (b) Acceleration

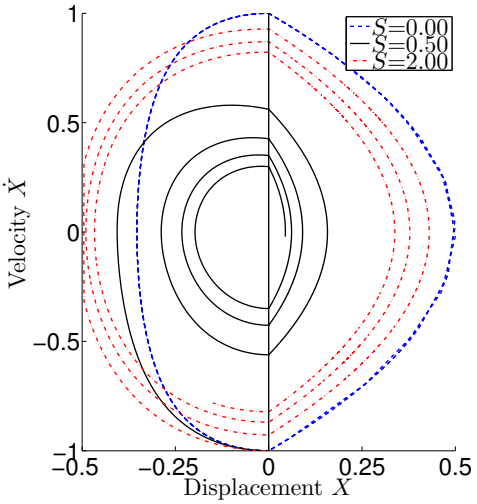

(c) Phase Portrait

Figure 4.4: Varying Area Ratio S

Figure 4.4 shows the responses as the area ratio S is varied. Since $S = 0$ is the case when the orifice is fully closed, the displacement response shows no damping – as seen in the phase portrait there is no decay. At $S = 2$, there is low damping as indicated by a spiral than converges less than the default case. As S increases further the response approaches the case where the orifice is the

size of the piston, the volume is the whole cylinder, and there is no corresponding damping. In this case, the response would be the same magnitude as the $S = 0$ case but with a longer period, which is what we see. It can be seen that the most damped response is for $S = 0.5$. However, optimization is required to find the value of S to produce the highest damping.

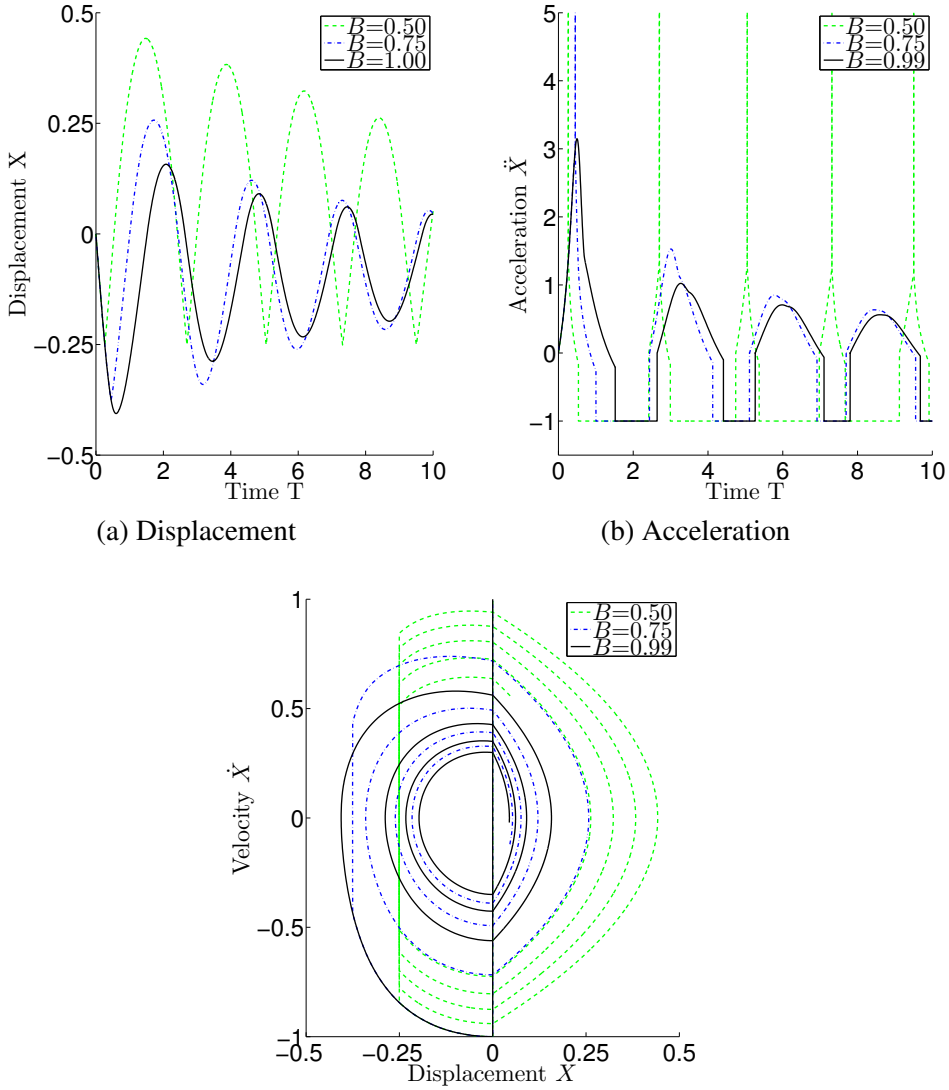

(a) Displacement

(b) Acceleration

(c) Phase Portrait

Figure 4.5: Varying Bellows Area Ratio B

Figure 4.5 shows the effect of having a small bellows area ratio B. Lower ratios mean more residual gas is left in CV1 when the bellows bottoms out. There are no other effects in the response that can be seen by the initial response: all values of B follow the same path until each bottoms out. The bottoming out can be seen in the displacement plot by a sharp v which corresponds to the impact at $X = -BV_{10}$, of course the acceleration is very large at that point also. The peaks are arbitrary since the spring stiffness once bottomed out was chosen simply as large to allow the numerical integration to run quickly, and is justified by deciding that bottoming out the bellows is not permissible so the response afterwards is not important. Bottoming out can also be seen clearly as vertical lines in the phase portrait, showing a sharp change in velocity while at the displacement where it bottoms out. In the cases shown here, the only response that does not bottom out initially is the nominal value $B = 1$. However, for $B = 0.75$ the second impact does not bottom out which shows there may be a value $0.75 < B < 1$ that does not bottom out.

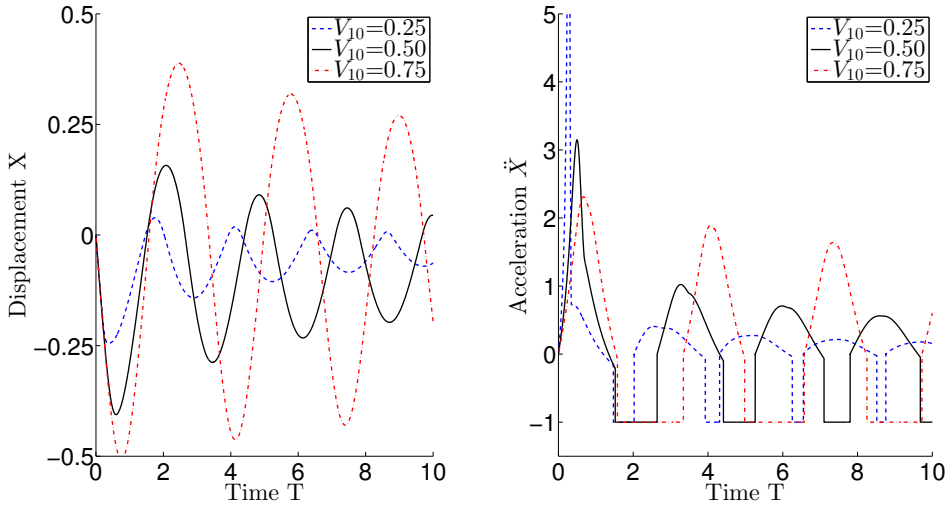

(a) Displacement

(b) Acceleration

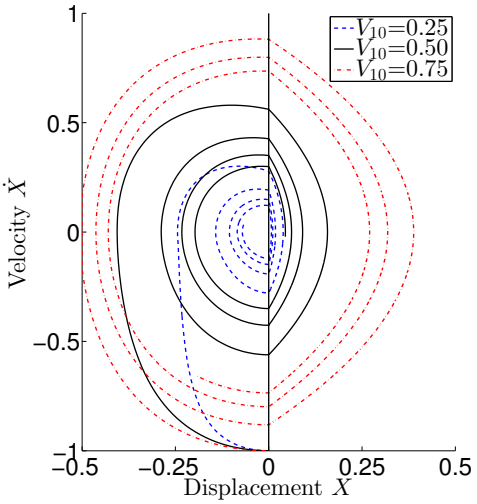

(c) Phase Portrait

Figure 4.6: Varying Initial Volume Ratio V_{10}

Figure 4.6 shows the effect of varying the initial volume ratio V_{10}. The nominal case $V_{10} = 0.5$ means CV1 and CV2 begin with equal values. When $V_{10} = 0.25$ there is less volume in CV1 so the stiffness is higher and the acceleration is higher. It can be seen in the displacement response that the device very nearly bottoms out, which would happen at $X = BV_{10} = 0.25$. This response

is also more damped than the other cases, which can be seen in the phase portrait having a spiral that tends towards equilibrium the quickest.

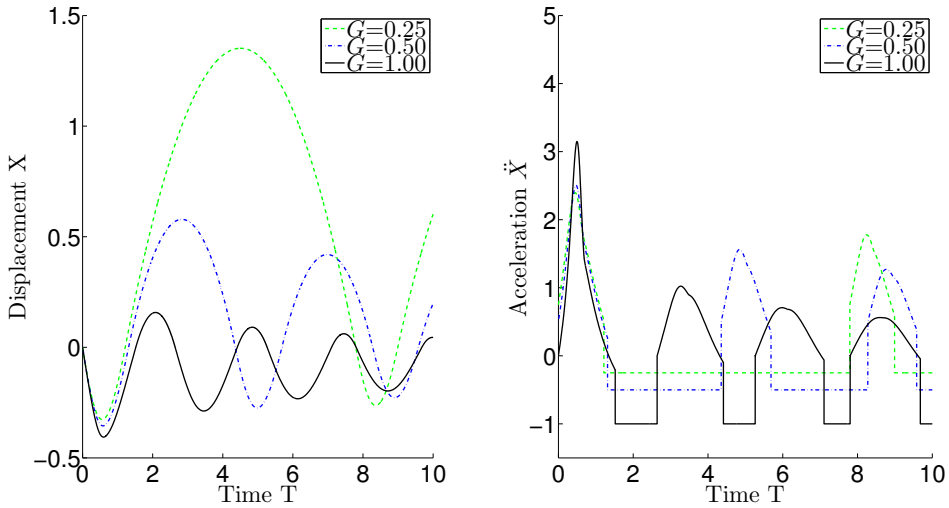

(a) Displacement

(b) Acceleration

(c) Phase Portrait

Figure 4.7: Varying Gravity G

Figure 4.7 shows the response for varying gravity G. Similar to the effect of varying mass, increasing gravity causes a larger displacement in the first cycle. Compared to the effect of varying mass,

the effect of varying gravity is more pronounced after the device leaves contact with the surface. As gravity is reduced, the bounce is higher and has a longer duration, a characteristic of landing on a low gravity planetary body. Leaving contact with the surface may yield a long distance travel before recontact. It should be noted here that this analysis uses the assumption that gravitational acceleration is constant since the goal was to model what happens during contact. For a very low gravity body, this assumption is not valid and the model of gravity falling off with distance squared should be used if one is interested in the actual bounce trajectory or orbit.

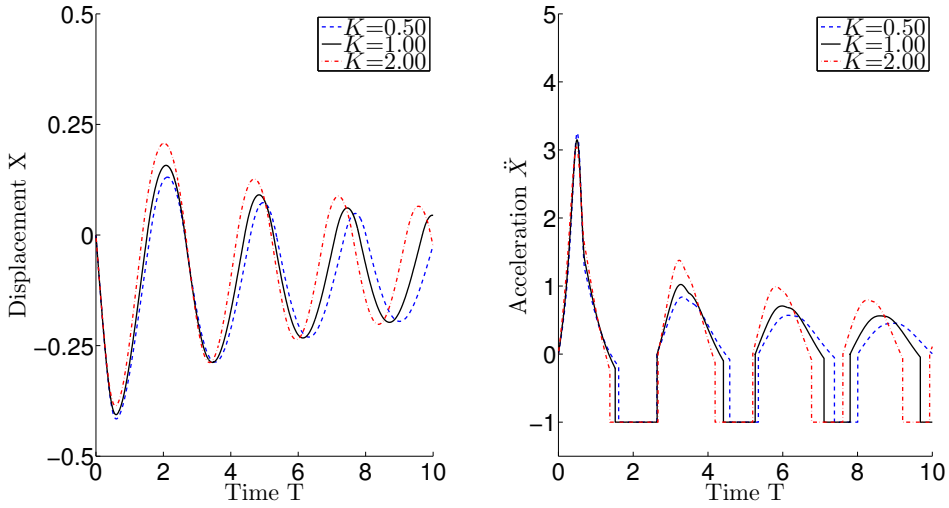

(a) Displacement (b) Acceleration

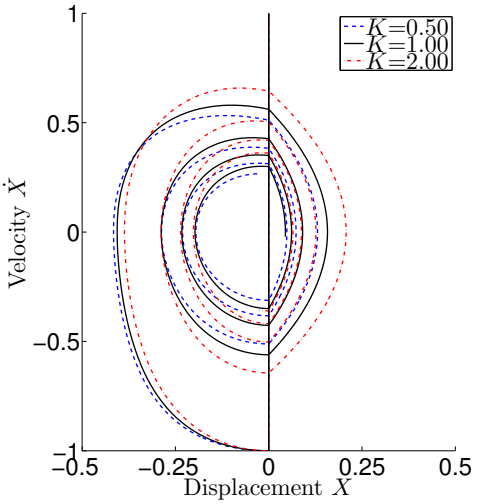

(c) Phase Portrait

Figure 4.8: Varying Bellows Stiffness K

Figure 4.8 shows the response to varying stiffness K. As expected, lower stiffness values result in larger displacement responses and longer periods. At least for the nominal parameter values the change in stiffness does not produce a large change in response. The reason for this lack of sensitivity is likely due to the force from the dimensionless pressure, which is significantly larger

than the dimensionless stiffness. In addition, the lower stiffness has higher damping, due to less energy stored in the spring and more non-conservative work done on the gas.

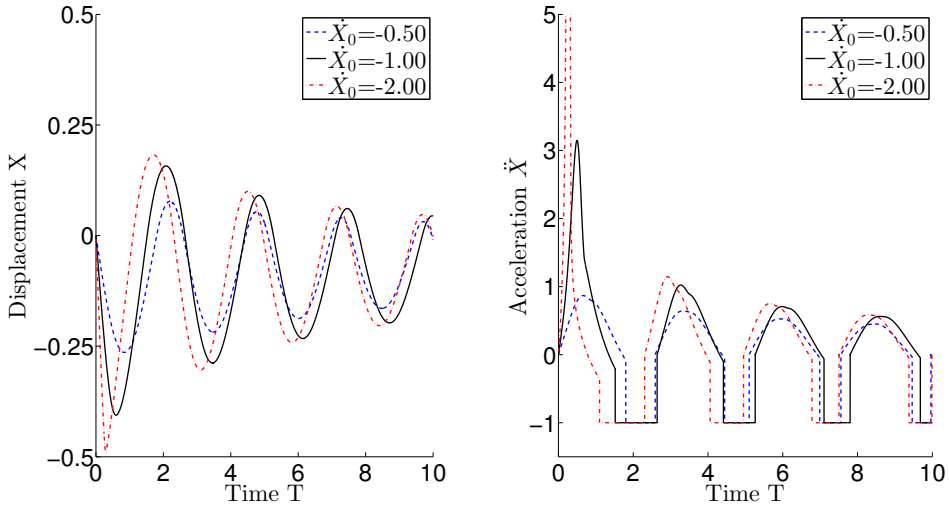

(a) Displacement (b) Acceleration

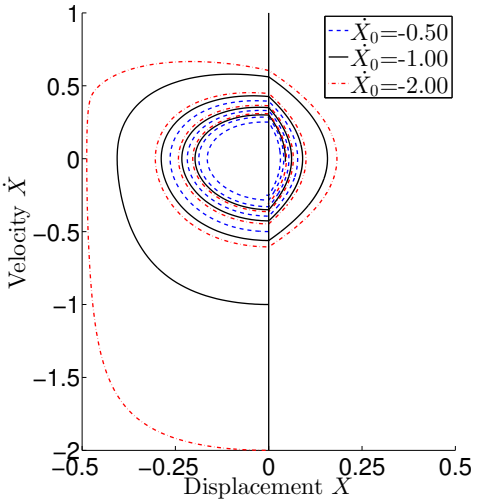

(c) Phase Portrait

Figure 4.9: Varying Initial Velocity $\dot{X}_0$

Figure 4.9 shows the response to varying the initial impact velocity $\dot{X}_0$. As expected, faster initial velocities lead to greater compression and require higher acceleration to stop the mass. The more

interesting finding is that the damping increases as the initial impact velocity increases so that, after a couple of cycles the responses are similar in magnitude. This increased damping is very noticeable for the cases of $\dot{X}_0 = 1$ and $\dot{X}_0 = 2$ where the height of the initial bounces are nearly identical. Impact velocity is a parameter that will certainly vary during a mission; this analysis shows that if the parameters are selected for the maximum velocity, the device will have similar long term responses at lower velocities.

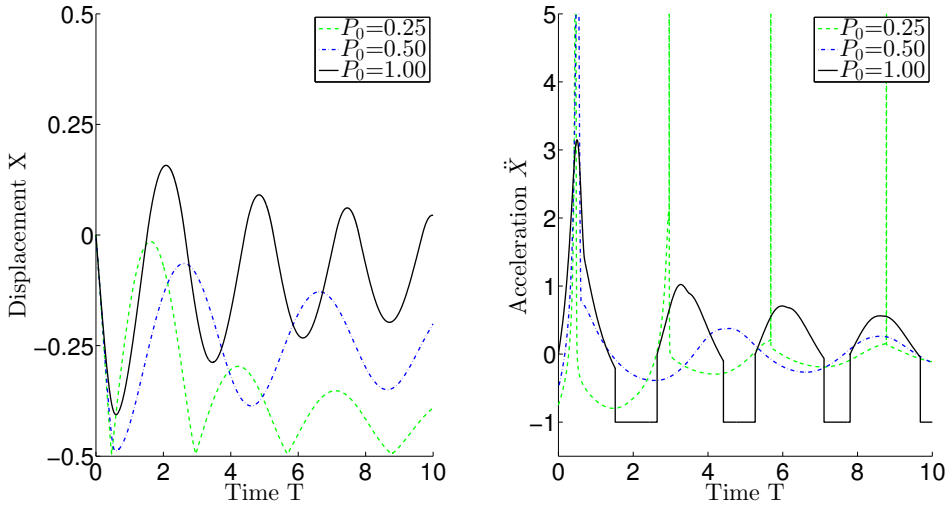

(a) Displacement (b) Acceleration

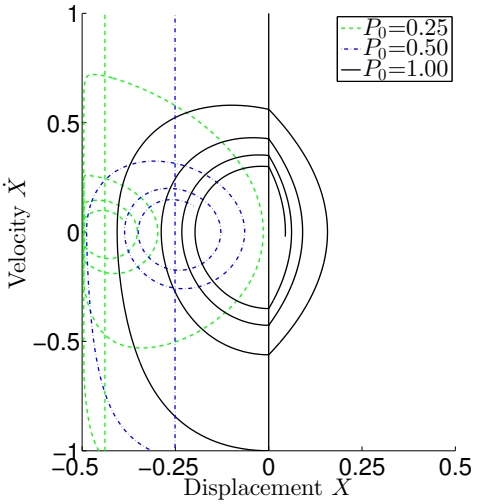

(c) Phase Portrait

Figure 4.10: Varying Initial Pressure P_0

Figure 4.10 shows the response while varying the initial pressure P_0. The results are fairly straightforward. Higher pressures result in less compression. In the case $P_0 = 0.25$, the device bottoms out. Lower initial pressures yields higher damping and lower static equilibrium values.

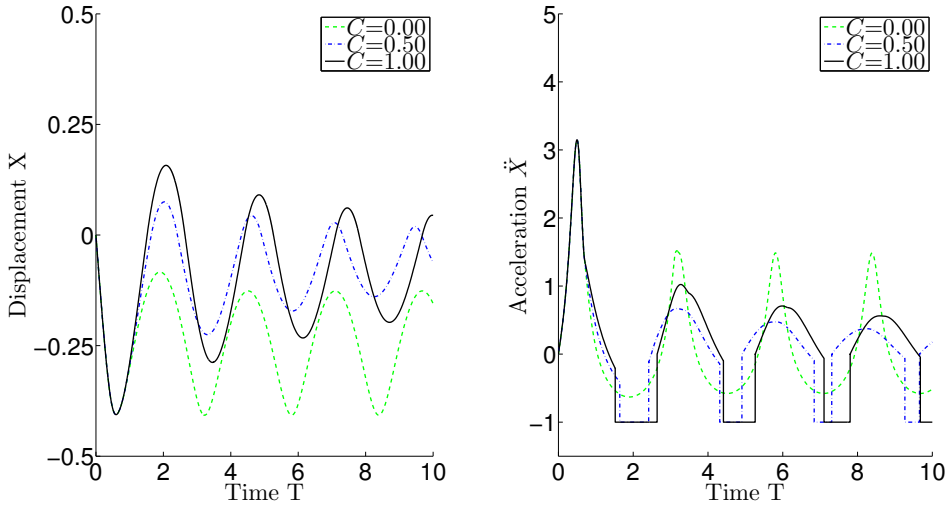

(a) Displacement (b) Acceleration

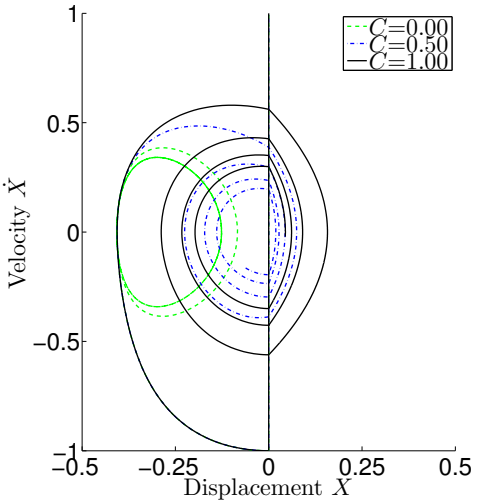

(c) Phase Portrait

Figure 4.11: Varying Check Valve Area Ratio C

Figure 4.11 shows the response when using a check valve where the return area is reduced by a fraction of the initial area. The case where $C = 0$ shows the smallest bounce but also the lowest damping because once the gas enters CV2, it can not leave so there is no damping. The case where $C = 1$ is the same as the default case. The highest damping from these plots is $C = 0.50$ which

has a small bounce but damps out quickly, however optimization would be required to find the value for C that produces the highest damping.

A general observation from all of these responses is that damping is higher when the initial response is close to bottoming out. This makes sense because gas flowing between the control volumes is what produces the damping and the flow is larger when the pressure ratio is higher.

The final variation is to simulate a hop by setting the parameters to the values shown in Table 4.2. The main difference compared to the nominal values is the initial position is bottomed out ($X_0 = -BV_{10}$) and the velocity is zero ($\dot{X}_0 = 0$). To simulate a hop by a valve opening, the initial pressure in CV1 is set to 1 ($P_{10} = 1$) and CV2 is set to a larger value to simulate the gas starting compressed to a higher value. The lowest simulated value ($P_{20} = 2$) is the maximum pressure P_2 reaches in the nominal case. The results are displayed in Figure 4.12 and as expected, higher pressures result in higher maximum altitudes. The nominal case barely leaves the surface which shows that for a relatively small orifice ($S = 0.5$) the system will experience damping on extension.

Table 4.2: Hop Parameters

Parameter	n	M	S	B	V_{10}	G	K	X_0	$\dot{X}_0$	P_{10}
Value	1.4	1	.5	1	.5	1	1	-0.5	0	1

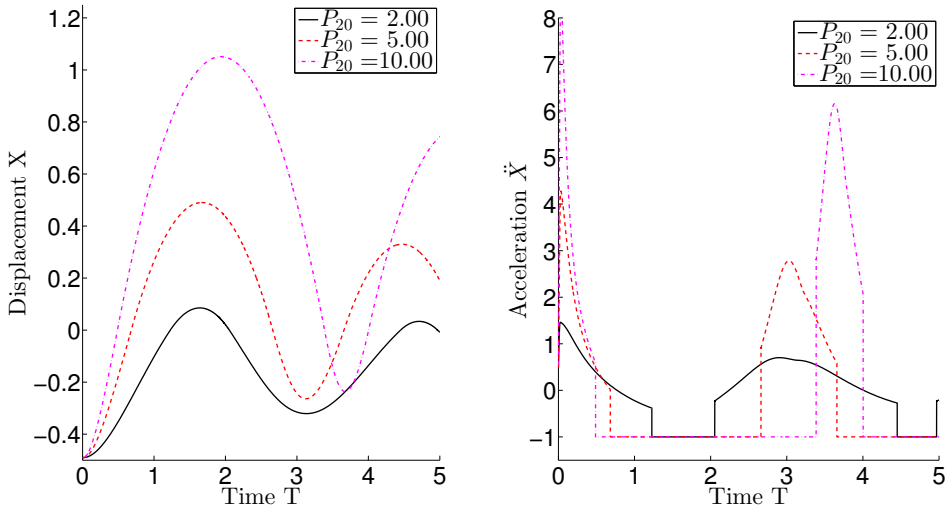

(a) Displacement (b) Acceleration

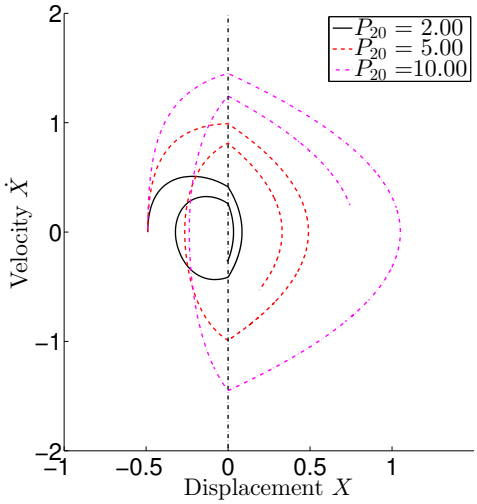

(c) Phase Portrait

Figure 4.12: Hopping

4.2 Initial Design Equations Verification

The initial design equations for static equilibrium and initial displacement bounds were compared to the results of the numerical integration. The parameter values were set to the default values with the exception of $V_{10} = 0.75$ and $P_0 = 0.6$. Then S was varied and the results are shown in Figure 4.13a. It can be seen that for the case where $S = 0.35$, the oscillations are converging on the static equilibrium value and the initial displacement is between the upper and lower bounds. When $S = 0$, the displacement reaches the upper bound and when $S = 4$ (or for any larger value) the displacement reaches the lower bound

The natural frequency estimate is used to determine how long to run a numerical analysis to include the desired number of cycles. To verify the natural frequency estimate, the default displacement response is shown in Figure 4.13b. Then error bars are drawn between the zero crossings of the plot and the period determined by the natural frequency estimate. In this case, the natural frequencies are overestimated, but are sufficiently accurate for the intended purpose.

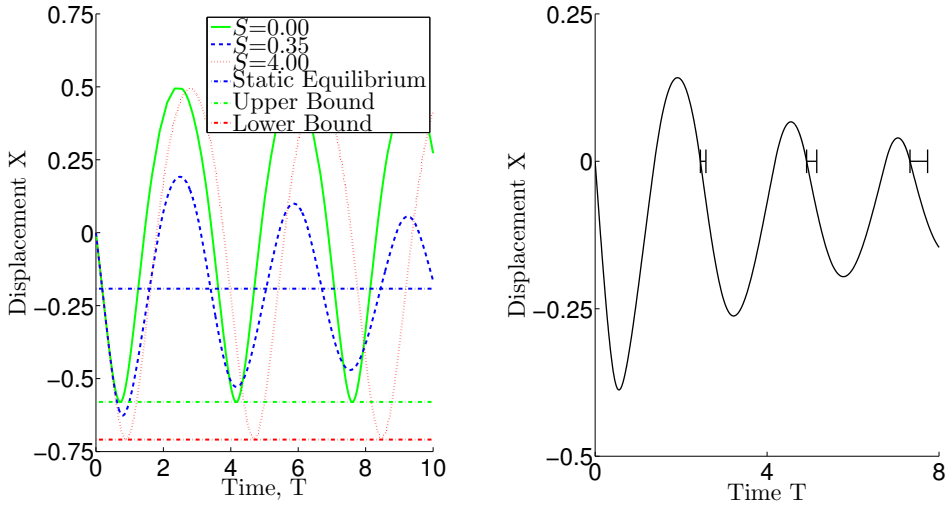

(a) Static Equilibrium and Stroke Bounds (b) Natural Frequency Estimate

Figure 4.13: Initial Design Equations Verification

4.3 On/Off Control

Active control requires choosing the system parameters such that the upper bound is above the static equilibrium, which is in turn above the stroke limit. In this example the two parameters that are able to be adjusted are P_0 and V_{10}. The upper bound, static equilibrium, and stroke limit were calculated for various values of P_0 and V_{10}. The points that failed the criteria were eliminated and the difference between the upper bound and the stroke limit are plotted in Figure 4.14a. The point selected was $P_0 = 0.4$ and $V_{10} = 0.51$.

On/Off control starts with the valve opened. Next, at some time T_1 the valve is closed when the the instantaneous upper bound is equal to the static equilibrium. Then, at some time T_2 near the steady state, the valve is opened allowing the pressures in the control volumes to equalize at the equilibrium. The actual times are found using optimization where the objective function

is to minimize the numerical integration of the difference between the response and the static equilibrium value. The results of this are shown in Figure 4.14b. Each line on the plot corresponds to a different initial velocity. Starting from the left with $\dot{X}_0 = -1$ to the right where $\dot{X}_0 = 0$. The individual points indicate T_1, or where the valve is first closed. The valves are opened very close to the static equilibrium and are omitted for clarity. Since T_1 and T_2 were solved numerically there is some error and the responses are brought to rest exactly at static equilibrium, which results in small long term oscillations.

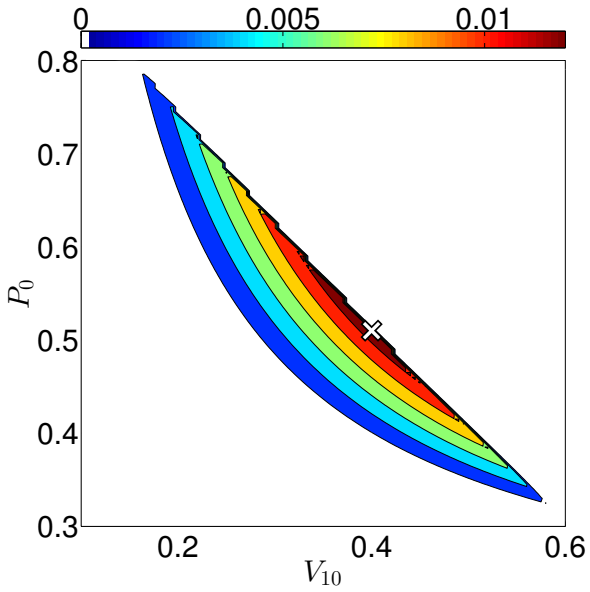

(a) Distance from Stroke Limit to Upper Bound

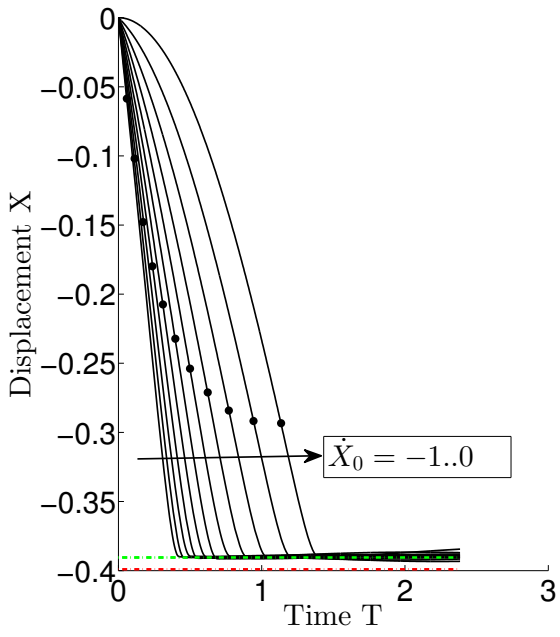

(b) On/Off Control Valve Timing

Figure 4.14: Active Control

4.4 Adaptive Control

The adaptive control uses the same parameter values as the On/Off control. In this analysis, the control is implemented in the differential equation file. Where the acceleration is calculated, it is checked against the control acceleration and the valve opening is set. Putting the control in the differential equation means that the control system has no lag, which is not realistic. In a real analysis the lag between taking measurements, performing calculations, adjusting outputs, and having the valve actually open and close would need to be determined and included in the model. Figure 4.15 shows that for all initial velocities the system follows an exponential decay towards static equilibrium, as desired.

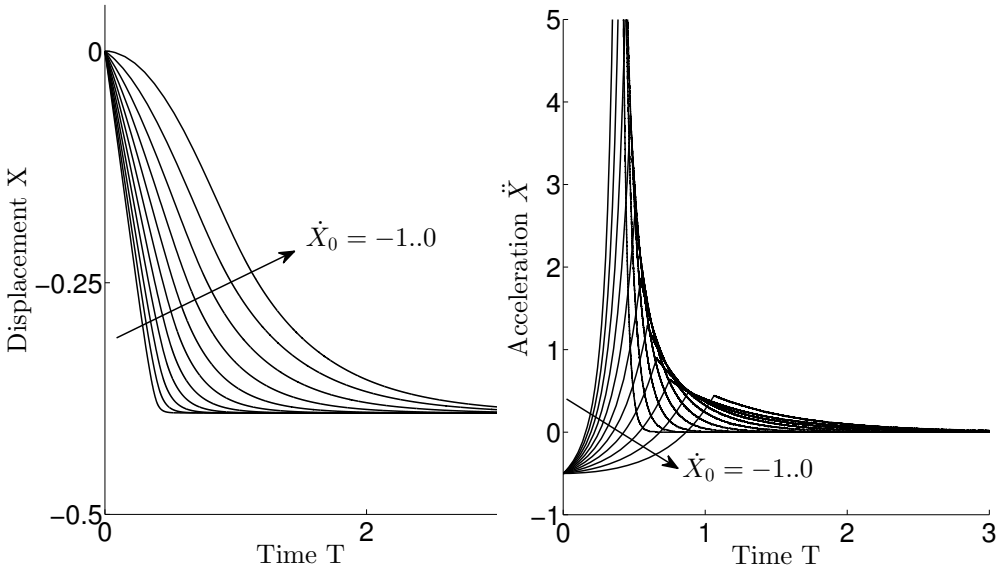

(a) Displacement (b) Acceleration

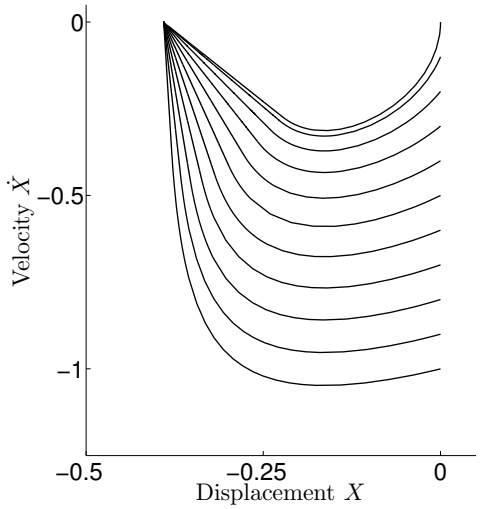

(c) Phase Portrait

Figure 4.15: Adaptive Control

4.5 Nondimensional Optimization

This example analysis will optimize the passive design with the assumed input parameters given in Table 4.3a and criteria given in Table 3.3. The variable parameters and their ranges are given in Table 4.3b. Since there are 4 parameters decreasing the step size will exponentially increase the run time. Preliminary runs with larger ranges and coarser resolution were run to find where the highest damping ratios were clustered. These ranges are a refinement of those runs. A MATLAB program was written to loop through all of the parameters and their ranges. A numerical simulation for each set of parameters was run for one period. The results were checked ensure the criteria were met. If so, a numerical simulation was run for ten periods and the damping model fit to the data as described in Section 3.5.1.

The results are sorted by damping ratio and the top five results are shown in Table 4.3c. Figure 4.16 shows the displacement and fit, acceleration curves, and phase portrait are shown for the first and fifth highest damping ratio. The displacement plots include the nonlinear fit line and their corresponding damping ratio. It can be seen that it relatively difficult to determine just from this plot which system has higher damping. The acceleration plots do not show much difference. The phase portrait provides the most insight in the plot with the higher damping ratio appears to converge to equilibrium more quickly. This helps verify the methodology used to select the objective function.

Table 4.3: Nondimensional Optimization Parameters

(a) Assumed

Parameter	Value
M	10
G	1
X_0	0
$\dot{X}_0$	-1
B	.9
n	1.4

(b) Optimized

Parameter	Range	Step Size
S	.1-.5	.05
V_10	.3-.6	.05
K	0-1	.1
P_0	.5 .9	.05

(c) Results sorted by ζ

S	V_{10}	K	P	A	B	ζ
0.25	0.50	0.0	0.65	0.163	0.007	0.232
0.25	0.50	0.1	0.65	0.166	0.007	0.227
0.25	0.55	0.2	0.60	0.177	0.008	0.207
0.30	0.40	0.1	0.80	0.104	0.010	0.193
0.30	0.40	0.0	0.80	0.119	0.011	0.187

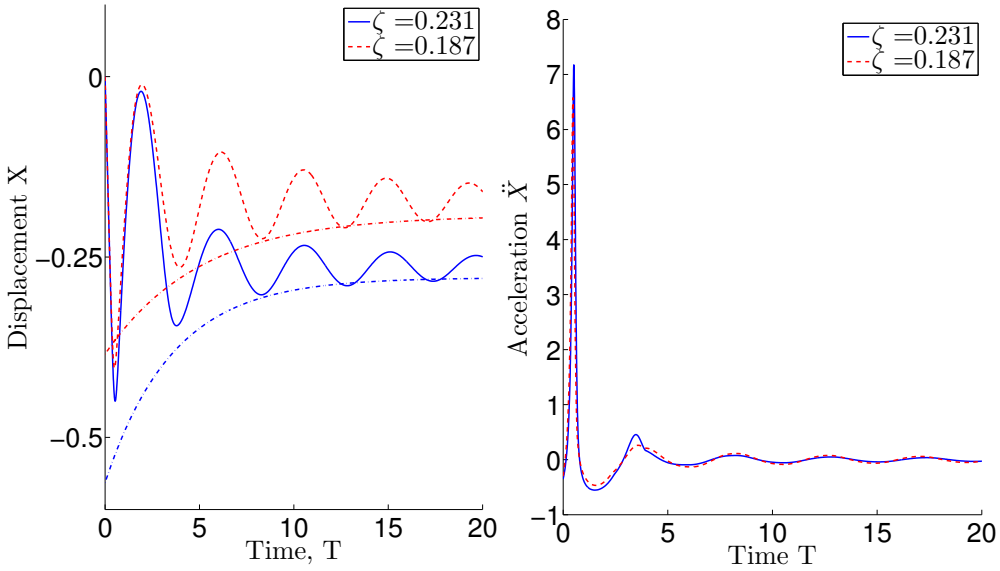

(a) Displacement (b) Acceleration

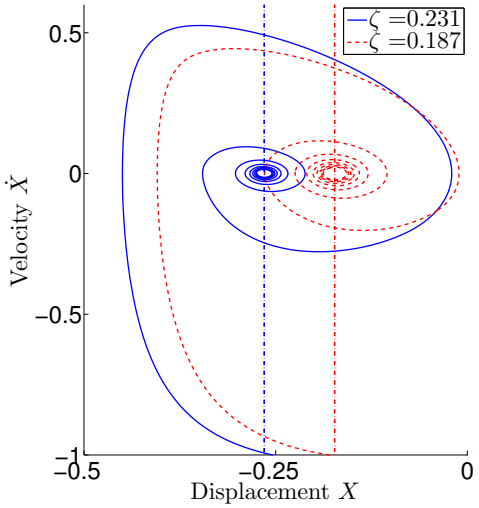

(c) Phase Portrait

Figure 4.16: Nondimensional Optimization

4.6 Optimization using Vendor Data

This analysis uses vendor provided data for the metal bellows to design the minimum mass shock absorber that meets the criteria in Table 4.4a. The vendor has a standard range of bellows capsules. The actuators are made by stacking and welding these capsules into the desired length. The data for the different sized bellows are given in Table 4.5.

Since the bellows parameters are now dimensional and all analysis has been nondimensional, values for the dimensional parameters need to be selected. These values are based on the environment, such as gravity and atmospheric pressure, and on the lander, such as mass, temperature, initial velocity, and position above the surface. Table 4.4b provides a summary where the inputs are chosen for a small hopper landing on the moon. The practical design, the designer of this subsystem will have control over stroke length l_s, initial pressure p_0, bellows spring rate k, and effective area of the bellows s. Not all of these parameters are independent; for example the bellows spring rate and maximum internal pressure will be related because the thickness of the bellows and number of convolutions will determine the stroke and maximum pressure the bellows can withstand. Since in the nondimensional analysis the choice of p_0 is arbitrary, it is set to the maximum allowable pressure for each bellows size, which allows for an additional nondimensional pressure criteria $P_1 > 1$.

Table 4.4: Dimensional Optimization Parameters

(a) Criteria

Criteria	Condition
No rebound	$max(X) \leq 0$
No Bottoming Out	$min(X) > -BV_{10}$
Max Pressure $<$ Allowable	$max(P_1) < 1$

(b) Inputs

Parameter	Value
g	$1.622\,\mathrm{m\,s^{-2}}$
m	$100\,\mathrm{kg}$
x_0	0
x_0'	$-1\,\mathrm{m\,s^{-1}}$
n	1.4
R	$288\,\mathrm{J\,kg^{-1}}$
θ_0	$300\,\mathrm{K}$
C_0	.7

(c) Results

Code	Capsules	V_{10}	P_0	S	ζ	mass (kg)
50	24	0.15	0.35	0.65	0.54	0.77
55	35	0.10	0.25	0.45	1.57	2.24
60	21	0.10	0.20	0.50	2.72	1.94
70	25	0.25	0.15	0.40	1.03	2.90
80	16	0.10	0.10	0.50	1.49	3.60

The optimization was performed in a manner similar to the nondimensional optimization, with the difference that the parameters need to be converted to nondimensional form. The program loops through each size bellows, adjusting the length by incrementing the number of capsules until an acceptable solution is found.

The results for the least number of capsules for the bellows that had solutions that met all criterai are shown in Table 4.4c. The responses for the two lightest configurations are shown in Table 4.4c and Figure 4.17. The larger bellows is 2.5 times heavier, but it has a damping ratio that is 5 times larger. Note that the mass is just that of the bellows, but seems appropriate for a 100 kg hopper.

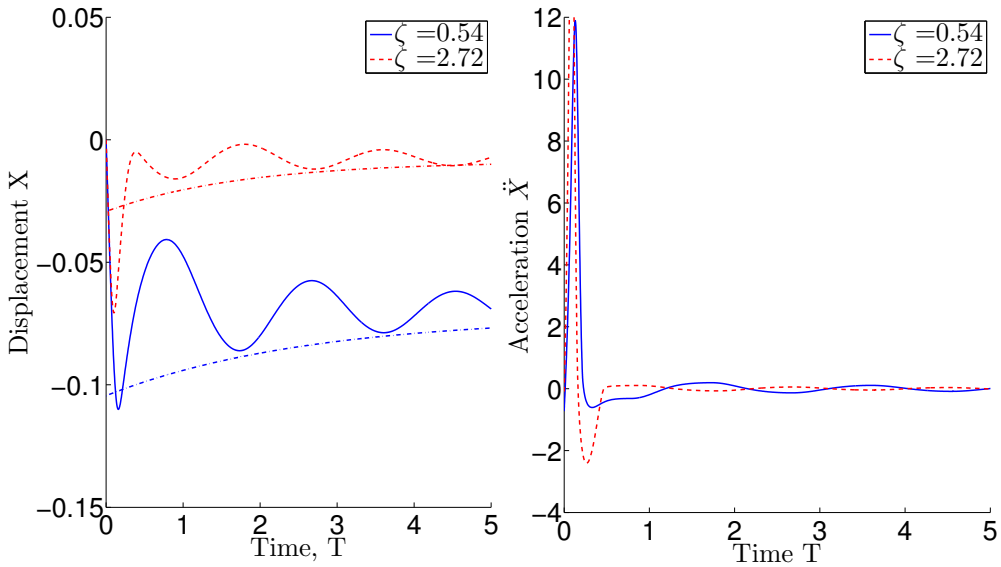

(a) Displacement

(b) Acceleration

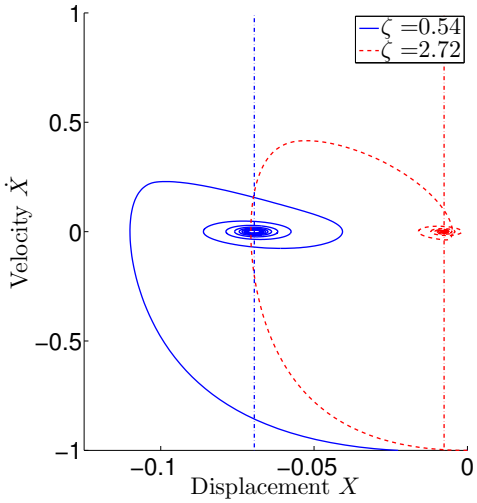

(c) Phase Portrait

Figure 4.17: Dimensional Optimization

Table 4.5: Metal Bellows Vendor Data From [31]

Code	D_o mm	D_i mm	A_e cm^2	P_{max} KPa	per capsule L_s mm	L_{max} mm	L_{min} mm	k_b N/mm
5	9.5	3.2	0.3	689	3.6	5.3	1.8	2.3
10	12.7	4.8	0.6	1034	8.4	11.7	3.3	9.6
20	19.0	6.4	1.3	345	7.6	9.9	2.3	4.2
30	26.2	14.0	3.2	207	13.5	16.8	3.3	4.4
35	38.1	24.6	7.7	276	7.4	10.9	3.6	3.9
40	41.4	19.0	7.1	297	7.9	10.9	3.0	2.1
50	48.0	35.3	13.6	310	21.8	26.7	4.8	2.6
55	57.2	38.1	17.7	345	12.7	18.3	5.6	3.7
60	64.8	44.4	23.4	345	18.0	24.6	6.6	4.7
70	75.9	50.8	31.6	276	23.9	29.7	5.8	5.1
80	101.3	68.3	56.5	276	25.4	31.8	6.4	8.8
85	108.0	81.3	71.0	310	20.3	28.7	8.4	13.1
90	126.2	101.6	101.9	345	20.3	29.2	8.9	13.1
93	177.3	126.5	181.3	172	25.4	30.2	4.8	7.4
95	279.4	241.3	532.1	138	25.4	29.0	3.6	43.8
98	457.2	406.4	1463.9	138	25.4	29.7	4.3	113.8

CHAPTER 5: CONCLUSION

The goal of this research was to prove the feasibility of using metal bellows shock absorbers to extend the range of hopper spacecraft by increasing landing velocity and initiating hops, thereby reducing the use of propellants. The work presented here shows this system can provide the performance required to land and launch a spacecraft on a planetary surface. More importantly, it has built upon the work already done in pneumatic damping and has provided methods and tools for further investigation.

5.1 Effective Area

The analysis of the effective area of the bellows shows that the industry estimation can have significant errors for bellows where the bellows area ratio is high. It should be noted that the triangular shaped bellows used in this analysis are not the only shape of bellows and if accurate effective area is required it should be calculated for the exact bellow geometry.

5.2 Equations of Motion

Nondimensional differential equations of motion and pressure were derived for a vacuum environment for the system impacting against a relatively stiff surface. The nondimensional bottoming out criteria was derived. The nondimensional static equilibrium was derived shown to equal 0 when the nondimensional parameters were normalized to 1. This can be used to select parameter relationships if a predetermined static equilibrium value is desired.

5.3 Analytical Estimations

Analytical solution for the bounds of stroke were found. These equations facilitate the initial sizing of a system, selecting parameter values for an active system, or tuning system parameters. The equations speed up calculations by providing a quick check if there will be a solution before running a computationally expensive numerical simulation.

The natural frequency estimate is provided to save optimization time and is shown to be sufficiently accurate for this purpose. Limiting the length of the numerical simulation can be especially helpful for systems that quickly damp out the numerical solver will adjust to very small time steps to provide the required accuracy. By limiting the run to the first few cycles, all of the criteria can be determined in a short amount of time.

5.4 Response to Parameter Variation

Intuition of the system was gained by varying the parameter values one at a time, in the range of interest, and visualizing the change in response. Some of these parameter values will be known a priori such as gravity and mass. Impact velocities are likely to change between each hop, but the analysis has shown, for a passive case, the system will perform well for velocities less than the maximum design velocity. The system designer has control over the remaining parameter values and can use this analysis to select values to meet system requirements.

One important parameter sensitivity had to do with the bellows area ratio B. This effects the residual volume in the cylinder. Damping is maximized as B approaches 1. The commercial bellows area ratios varied from .44 for the smallest bellows to .89 for the largest. The simulations show that low bellows ratios make it difficult to achieve high damping. At one point during optimization, B

was included as a parameter, but every optimal result was returned with $B = 1$ so it was discarded from further optimizations.

5.5 Control Concepts

The first control concept used a check valve to vary the orifice size depending on the pressure differential between the control volumes. This improved the damping performance with only mechanical flow controls.

The second control concept used an on/off valve to bring the system to rest with minimal oscillation. The valve was initially open and then closed at the time required for the system to come to rest at static equilibrium. Finally the valve would open slightly before coming to rest to allow time to vent the pressure so the system arrives at static equilibrium with near zero velocity. This analysis was done over all velocities. A polynomial could be fit to these timing values so that a control system could measure impact velocity and determine the required timing.

The final control concept used the current position and velocity to determine the exponential decay constants to reach static equilibrium at zero velocity. The instantaneous acceleration is compared to the required acceleration, and the valve is opened or closed as required.

All of these control concepts improved performance over the purely passive orifice system. Which concept is used would be based on system requirements. The passive system is the simplest, lightest, and requires no power. The check valve is only a mechanical addition and does not requires control or power. The on/off control requires power and control, but since it only turns on and off one time it requires less power than the adaptive control which is continuously operating.

5.6 Linear Equivalent Damping Coefficient for Nonlinear Response

A novel way of determining an equivalent damping coefficient was derived using the time integration of the absolute value of the distance from equilibrium, which proved to be a robust way to fit the model to the data. It successfully neglected the initial nonlinear spike and fit the entire response well. In addition the model provided a parameter for the magnitude of the long term oscillations about the static equilibrium that would exist if there was no friction on the system. This method was verified using an example of a viscous damped system with residual oscillation around static equilibrium and the parameters were recovered. Most importantly, maximizing the estimated damping coefficient was successfully used as the objective function for optimization.

5.7 Optimization

Two different optimizations were conducted. The first was for a passive case. Parameter values, that a designer would typically have control of, were allowed to vary to find a solution that produced maximum damping while meeting the criteria of not bottoming out and not rebounding off the surface.

The second optimization used dimensional parameter values to simulate a 100 kg lunar hopper and vendor provided bellows data. The data was nondimensionalized and each size bellows was incrementally increased in length and tested to ensure it met the criteria of not bottoming out, not rebounding, and not exceeding the allowable pressure. Then the configuration with the lowest mass of $0.77\,\mathrm{kg}$ was selected.

5.8 Future Work

Future work should include experiments to verify the models presented here. These should be conducted in a vacuum chamber and with gravity offload devices to simulate the types of planetary bodies hoppers would be used. Research should continue on ways to actively and semi-actively control the system. Effort should be put into designing a system to compress the gas in CV2 in a way that can be hermetically sealed and actuated with a high force, low power actuator to be used for powered hops. Valves that can be integrated into a sealed design need to be explored. Experiments should be conducted to determine if the actively controlling the valve as proposed here is feasible in practice.

APPENDIX A: ANDERSON NONLINEAR SPRING

A.1 MATLAB: Section4_7diff.m

```
clear all;
close all;

x0=linspace(-2.4,.9,100);
dx0=0;
n=[1 1.4 1.66];

[t,y]=ode45(@Section4_7ODE,[0 20],[0 -.5],[],1.4);

for i=1:length(n)
    for j=1:length(x0)
        [t,y]=ode45(@Section4_7ODE,[0 20],[x0(j) dx0],[],n(i));
%         y(:,3)=-1/n*(1./(1-y(:,1)).^n-1)
figure(1)
hold on
plot(y(:,1),y(:,2))
% legend('Pos','Vel','Acc')
        Xmax(j)=max(y(:,1));
        Xmin(j)=min(y(:,1));
        Vmax(j)=max(y(:,2));
        Xzero=fzerodiscrete(t,y(:,1));
        Vzero=fzerodiscrete(t,y(:,2));
        Per(j)=Vzero(3);
        QPerI(j)=Xzero(2)-Vzero(2);
        QPerD(j)=Vzero(1);
    end
    figure(2)
```

```
    subplot(3,1,1)
    axis([0 2 0 2.4])
    hold on;
    plot(Vmax,Xmax);
    plot(Vmax,-Xmin);
    plot([0 2],[0 2])

    subplot(3,1,2)
    axis([0 2 6 9])
    hold on;
    plot(Vmax,Per)
    line([0 2.0],[pi*2 pi*2])

    subplot(3,1,3)
    axis([0 2 0 4])
    hold on;
    plot(Vmax,QPerI)
    line([0 2.0],[pi/2 pi/2])
end
```

A.2 MATLAB: Section4_7ODE.m

```
function dx=Section4_7ODE(t,x,n);
    dx=zeros(2,1);%This is a pre-initialization.
    %x(1)= Position
    %x(2)= Velocity
    dx(1)= x(2);% Velocity
    dx(2)= -1/n*(1/(1-x(1))^n-1); % Acceleration
end
```

APPENDIX B: OBJECTIVE FUNCTION DEMONSTRATION

B.1 MATLAB: Objective_Function_Demonstration.m

```
% John Trautwein jktrautwein@gmail.com  2015/10/14
clear all
close all

% Time Series
t=0:.01:10;

% Damping ratio
zeta=.2;
% Non zero limit
offset=.01;

% Model Data Exponential Decay to non zero value
x=sin(pi*t).*(exp(-zeta*t)+offset);

% Cumulative Trapazoid Integration of abs(x)
sum=cumtrapz(t,abs(x));

% Model Function
modelFun=@(b,t) cumtrapz(t,b(1)*(exp(-b(2)*t)+b(3)));

% Start values
start=[.1 .1 .1];

% Nonlinear fit
nlm=fitnlm(t,sum,modelFun,start);
```

```
% Coefficient Estimates
b=nlm.Coefficients.Estimate;

% Plots
figure('Position',[0 0 1000 1000])
hold all

% Abs Position Data from Steady State
plot(t,abs(x),'b','LineWidth',2)

% Cumulative Integration
plot(t,sum,'b','LineWidth',2)

% Model fit to Cumulative Integration
plot(t,cumtrapz(t,b(1)*(exp(-b(2)*t)+b(3))),'r--','LineWidth',2)

% Analytical Fit to Peaks with fit parameters
plot(t,pi/2*b(1)*(exp(-b(2)*t)+b(3)),'r--','LineWidth',2)

ftsz=36;
xlabel('Time, T','FontSize',ftsz); ylabel('Displacement X','FontSize',ftsz)
axis([0 10 0 5])
set(gca,'XTick',[0 2 4 6 8 10])
set(gca,'YTick',[0 1 2 3 4 5])
set(gca,'FontSize',ftsz)
Leg_st=legend('$ \left| \sin(\pi*t)e^{-0.2*t}+0.1 \right|$',...
        '$\int \left| \sin(\pi*t)e^{-0.2*t}+0.1 \right| dt$',...
        '$\int \left| A e^{-\zeta*t}+B \right| dt$',...
        '$\frac{\pi}{2}A e^{-\zeta t}+B$');
h= legend(Leg_st);
set(h,'Interpreter','latex')
```

APPENDIX C: RESPONSE TO PARAMETER VARIATION

C.1 MATLAB: Dimensionless_Damped_Bellows_D.m

```
% John Trautwein jktrautwein@gmail.com  2015/10/14
% Calculated and Plots Displacement, Velocity, and Acceleration for
% impact with surface for parameter variation

clear all;
close all;

% System non dimensional Parameters
% Put varied Parameter values in [] for only one parameter
n=  1.4;% Ratio of specific heats
M=  1;  % Moving Mass
S=  .5; % Area Ratio
B=  .99;% Bellows Ratio (effective area/cylinder area)
V10=.5; % Volume Ratio
G=  1;  % Gravity
K=  1;  % Bellows Stiffness
X0= 0;  % Position
Xd0=-1; % Velocity
P0= 1;  % Pressure
T0= 0;  % Valve Open Time
C=  1;  % Check Valve %S
ts= 10; %Simulation Time
Kb= 1e6;% Bellows Bottom Out Stiffness

%x(1)= X
%x(2)= Xd
%x(3)= P1
```

```
%x(4)= P2

% Create Figures
figure('Position',[0 0 1000 1000])
figure('Position',[0 0 1000 1000])
figure('Position',[0 0 1000 1000])
figure('Position',[0 0 1000 1000])

% Set Plot Line color and values
ftsz=36;
LinSt={'-', '-', ':', '-.'};
LinCl={'k','k','r','g'};

% Loop for the variable under consideration
for i=1:length(M)

% Run ODE
% ***Insert (i) after varied parameter***
opt = odeset('RelTol',1e-14);
[t,y]=ode45(@Dimensionless_Damped_Bellows_ODE,[0 ts],...
            [X0 Xd0 P0 P0],[opt],M(i),K,Kb,G,n,V10,S,T0,B,C);

X=  y(:,1);
Xd= y(:,2);
P1= y(:,3);
P2= y(:,4);

% Calculate D
D=X;
D(D>=0)=0;
```

```
% Calculate Acceleration
% ***Insert (i) after varied parameter***
Xdd = ((X<=0).*(P1-K.*D)-(X<=-B*V10).*Kb.*(B*V10+D)-M(i).*G)./M(i);

% Plot Figures
figure(1)
hold all
plot(t,X,'LineWidth',2,'Color',LinCl{i},'LineStyle',LinSt{i})

figure(2)
hold all
plot(t,Xd,'LineWidth',2,'Color',LinCl{i},'LineStyle',LinSt{i})

figure(3)
hold all
plot(t,Xdd,'LineWidth',2,'Color',LinCl{i},'LineStyle',LinSt{i})

figure(4)
hold all
plot(X,Xd,'LineWidth',2,'Color',LinCl{i},'LineStyle',LinSt{i})

% Calculate Steady State
% ***Insert (i) after varied parameter***
SteadyState=@(Dv)P0./(1+Dv).^n-K.*Dv-M(i)*G;
Xss(i)=fzero(SteadyState,-V10/2);
end

% Legend Creattion
% ***Insert Parameter to include in Legen***
Leg_st=strcat('$C$=',cellstr(num2str(C', '%.2f')));
```

```
set(0,'DefaultTextInterpreter', 'latex')

figure(1)
    xlabel('Time T','FontSize',ftsz);
    ylabel('Displacement X','FontSize',ftsz)
    axis([0 ts -.5 .5])
    set(gca,'XTick',[0 2 4 6 8 10])
    set(gca,'YTick',[-.5 -.25 0 .25 .5])
    set(gca,'FontSize',ftsz)

figure(2)
    xlabel('Time T','FontSize',ftsz);
    ylabel('Velocity $\dot{X}$','FontSize',ftsz)
    axis([0 ts -1 1])
    set(gca,'FontSize',ftsz)

figure(3)
    xlabel('Time T','FontSize',ftsz);
    ylabel('Acceleration $\ddot{X}$','FontSize',ftsz)
    axis([0 ts -1.5 5])
    set(gca,'XTick',[0 2 4 6 8 10])
    set(gca,'FontSize',ftsz)

figure(4)
   hold all
   ylabel('Velocity $\dot{X}$','FontSize',ftsz);
   xlabel('Displacement $X$','FontSize',ftsz)
   axis([-.5 .5 -1 1 ])
   set(gca,'XTick',[-.5 -.25 0 .25 .5])
   set(gca,'YTick',[-1 -.5 0 .5 1])
   set(gca,'FontSize',ftsz)
```

```
    for i=1
        plot([Xss(i) Xss(i)],[-1 1],'LineWidth',2,...
            'Color',LinCl{i},'LineStyle',LinSt{i})
    end
```

C.2 MATLAB: Dimensionless_Damped_Bellows_ODE.m

```
function dx=Dimensionless_Damped_Bellows_ODE(T,x,M,K,Kb,G,n,V10,S,T0,B,C)
    dx=zeros(4,1);

    % Parameters
    V2 = 1-V10;
    X=x(1);
    Xd=x(2);
    P1 = x(3);
    P2 = x(4);

    % Valve Closed
    if T<T0
        S=0;
    end

    % Check for Choked Flow
    Pu=max([P1 P2]);
    Pd=min([P1 P2]);

    % Calculate C2
    if Pu/Pd > ((n+1)/2)^(n/(n-1))
```

```
    C2= sqrt(n/(((n+1)/2 )^((n+1)/(n-1))));
else
    C2= (Pd/Pu)^(1/n)*sqrt((2*n/(n-1))*(1-(Pd/Pu)^((n-1)/n)));
end

% Contact Base Input
if X<=0
   D=X;
   Dd=Xd;
else
   D=0;
   Dd=0;
end

% Equation of Motion
Xdd = ((X<=0)*(P1-K*D)-(X<=-B*V10)*Kb*(B*V10+D)-M*G)/M;

% Pressure Diferential Equations
if P2>P1
   S=C*S;
   P1d=(C2*S*P1^((n-1)/n)*P2^((n+1)/(2*n))-n*Dd*P1)/(V10+D);
   P2d= -C2*S*P2^((3*n-1)/(2*n))/V2;
else
   P1d=(-C2*S*P1^((3*n-1)/(2*n))-n*Dd*P1)/(V10+D);
   P2d= C2*S*P2^((n-1)/n)*P1^((n+1)/(2*n))/V2;
end

% Differentials
dx(1)=Xd;
dx(2)=Xdd;
dx(3)=P1d;
```

```
    dx(4)=P2d;

end
```

APPENDIX D: INITIAL DESIGN EQUATIONS

D.1 MATLAB: Dimensionless_Damped_Bellows_SS_Bound.m

```
% John Trautwein jktrautwein@gmail.com  2015/10/14
% Calculated and Plots Displacement with steady staet and Stroke Limits

clear all;
close all;

% System non dimensional Parameters
n=  1.4;        % Ratio of specific heats
M=  1;          % Moving Mass
S=  [0 .35 4];  % Area Ratio
B=  .99;        % Bellows Ratio (effective area/cylinder area)
V10=.75;        % Volume Ratio
G=  1;          % Gravity
K=  1;          % Bellows Stiffness
Kb= 1e6;        % Bellows Bottom Out Stiffness
T0= 0;          % Valve Open Time
C=  1;          % Check Valve %S

% Initial Values
X0= 0;          % Position
Xd0=-1;         % Velocity
P0= .6;         % Pressure
ts= 10;         % Simulation Time

%x(1)= X
%x(2)= Xd
%x(3)= U
```

```
%x(4)= P1
%x(5)= P2

figure('Position',[0 0 1000 1000])
LinSt={'-', '--', ':', '-.'};
LinCl={'g','b','r',[.5 0 1]}

for i=1:length(S)

% Run ODE
opt = odeset('RelTol',1e-14);
[t,y]=ode45(@Dimensionless_Damped_Bellows_ODE,[0 ts],...
      [X0 Xd0 P0 P0],[opt],M,K,Kb,G,n,V10,S(i),T0,B,C);

X=  y(:,1);
Xd= y(:,2);
P1= y(:,3);
P2= y(:,4);

% Calculate D
D=X;
D(D>=0)=0;

% Calculate Acceleration
Xdd = ((X<=0).*(P1-K.*D)-(X<=-B*V10).*Kb.*(B*V10+D)-M.*G)./M;

figure(1)
hold all
plot(t,X,'LineWidth',3,'Color',LinCl{i},'LineStyle',LinSt{i})
end
```

```
% Calculate Steady State
SteadyState=@(Dv)P0./(1+Dv).^n-K.*Dv-M*G;
Xss=fzero(SteadyState,-V10/2);

% Calculate Stroke Limits
% Change in Kinetic Energy
KE=1/2*M*Xd0^2;
% Change in Potential Gravitational Energy
PE=@(Dv)M*G*(X0-Dv);
% Change in Potential Spring Energy
SE=@(Dv)1/2*K*Dv.^2;
% Compression work for lower limit
PWl=@(Dv)(P0/(1-n))*((1+Dv).^(1-n)-1);
% Compression work for upper limit
PWu=@(Dv)(P0*V10^n/(1-n))*((V10+Dv).^(1-n)-V10^(1-n));

% Solve for Stroke Limits
Xsl=fzero(@(Dv) KE+PE(Dv)-SE(Dv)+PWl(Dv),-V10/2);
Xsu=fzero(@(Dv) KE+PE(Dv)-SE(Dv)+PWu(Dv),-V10/2);

% Plot Steady State and Stroke Limits
plot([0 ts],[Xss Xss], 'b-.','LineWidth',3)
plot([0 ts],[Xsu Xsu], 'g-.','LineWidth',3)
plot([0 ts],[Xsl Xsl], 'r-.','LineWidth',3)

% Configure Plots
set(0,'DefaultTextInterpreter', 'latex')
Leg_st=strcat('$S$=',cellstr(num2str(S', '%.2f')));
Leg_st(4)=cellstr('Steady State');
Leg_st(5)=cellstr('Upper Limit');
Leg_st(6)=cellstr('Lower Limit');
```

```
ftsz=36;

xlabel('Time, T','FontSize',ftsz);
ylabel('Displacement X','FontSize',ftsz)
axis([0 ts -.75 .5])
set(gca,'XTick',[0 2 4 6 8 10])
set(gca,'YTick',[-.75  -.5 -.25 0 .25 .5])
set(gca,'FontSize',ftsz)
h= legend(Leg_st);
set(h,'Interpreter','latex')
```

D.2 MATLAB: Dimensionless_Damped_Bellows_Natural_Freq.m

```
% John Trautwein jktrautwein@gmail.com  2015/10/14
% Calculated and Plots Natural Frequency Estimate

clear all;
close all;

% System non dimensional Parameters
n=  1.4;        % Ratio of specific heats
M=  1;          % Moving Mass
S=  .35;  % Area Ratio
B=  .99;        % Bellows Ratio (effective area/cylinder area)
V10=.5;        % Volume Ratio
G=  1;          % Gravity
K=  0;          % Bellows Stiffness
Kb= 1e6;        % Bellows Bottom Out Stiffness
T0= 0;          % Valve Open Time
```

```
C=  1;          % Check Valve %S

% Initial Values
X0= 0;          % Position
Xd0=-1;         % Velocity
P0= 1;         % Pressure
ts= 10;         % Simulation Time

%x(1)= X
%x(2)= Xd
%x(3)= U
%x(4)= P1
%x(5)= P2

% Natural Frequency Estimate
omega=(1/2/pi)*sqrt((n*P0/V10+K)/M);
ts=4/omega;

% Run ODE
opt = odeset('RelTol',1e-14);
[t,y]=ode45(@Dimensionless_Damped_Bellows_ODE,[0 ts],...
      [X0 Xd0 P0 P0],[opt],M,K,Kb,G,n,V10,S,T0,B,C);

X=  y(:,1);
Xd= y(:,2);
P1= y(:,3);
P2= y(:,4);

% Calculate D
D=X;
D(D>=0)=0;
```

```
% Calculate Acceleration
Xdd = ((X<=0).*(P1-K.*D)-(X<=-B*V10).*Kb.*(B*V10+D)-M.*G)./M;

% Calculate index of X zero crossing
ind=1:length(X)-1;
inz=find ((X(ind)>0 & X(ind+1)<0) | (X(ind)<0 & X(ind+1)>0));

% Calculate Actual and estimated natural frequency
t_a=t(inz(2:2:end));
t_e=[1:5]'*ts/5;

% Plot Results
figure('Position',[0 0 1000 1000])
hold all
plot(t,X,'k','LineWidth',2);
set(0,'DefaultTextInterpreter', 'latex')
Leg_st=strcat('$M$=',cellstr(num2str(M', '%.2f')));
ftsz=36;
xlabel('Time T','FontSize',ftsz); ylabel('Displacement X','FontSize',ftsz)
axis([0 8 -.5 .25])
set(gca,'XTick',[0  4 8 12])
set(gca,'YTick',[-.5 -.25 0 .25 .5])
set(gca,'FontSize',ftsz)

% Plot x error bars
plot([t_e t_e],[-.02 .02],'k','LineWidth',2)
plot([t_a t_a],[-.02 .02],'k','LineWidth',2)
plot([t_a t_e],[0 0],'k','LineWidth',2)
```

APPENDIX E: CONTROL CONCEPTS

E.1 MATLAB: Dimensionless_Damped_Bellows_On_Off.m

```
% John Trautwein jktrautwein@gmail.com  2015/10/14
% Use to Find T1 and T2 to being system to rest at steady state

clear all;
close all;

% System non dimensional Parameters
n=  1.4;    % Ratio of specific heats
M=  1;      % Moving Mass
S=  4;      % Area Ratio
B=  .95;    % Bellows Ratio (effective area/cylinder area)
V10=.42;    % Volume Ratio
G=  1;      % Gravity
K=  0;      % Bellows Stiffness
Kb= 1e6;    % Bellows Bottom Out Stiffness

optODE  = odeset('RelTol',1e-12);
optfmin = optimset('Display','off','DiffMinChange',.001);

% Initial Values
X0= 0;          % Position
Xd0= -1:.1:0;   % Velocity
P0= .5;         % Pressure

% Find Steady State
SteadyState=@(Dv)P0./(1+Dv).^n-K.*Dv-M*G;
Xss=fzero(SteadyState,-V10/2);
```

```
% Time Increment
inc=.001;

for iX=1:length(Xd0)

    % Time of Simulation set to half period
    ts=inv((1/2/pi)*sqrt((n*P0/V10+K)/M));

    % Nonlinear solver to find T1
    fun=@(T0) Min_T1_Find(T0,X0,Xd0(iX),P0,M,K,Kb,G,n,V10,S,B);
    T1=fzero(fun,.16,optfmin);

    % Run ODE with new T1
    [t,y]=ode45(@Dimensionless_Damped_Bellows_On_Off_ODE,[0 ts],...
          [X0 Xd0(iX) P0 P0],[optODE],M,K,Kb,G,n,V10,S,B,T1,ts);
    X=y(:,1);
    Xd=y(:,2);

    % Find index for zero crossings of Xd to pick T2 and trim ts.
    ind=1:length(Xd)-1;
    inz=find ((Xd(ind)>0 & Xd(ind+1)<0) | (Xd(ind)<0 & Xd(ind+1)>0));
    T2=t(inz(1));
    ts=t(inz(2));

    % Calculate trapazoid integration for minimization
    intc=trapz(t,abs(X-Xss));

    % Start T2 refinement - Loop until integration does not get better
    while 1
    % Decrement T2 by increment
```

```
    T2=T2-inc;
    % Run ODE
    [t,y]=ode45(@Dimensionless_Damped_Bellows_On_Off_ODE,[0 ts],...
    [X0 Xd0(iX) P0 P0],[optODE],M,K,Kb,G,n,V10,S,B,T1,T2);
    X= y(:,1);
    % Set prior integration to current
    intp=intc;
    % Calculate new current integration
    intc=trapz(t,abs(X-Xss));
    % Test for integration not improving
    if intc>intp, break, end
    end

    while 1
    % Increment T2 by 1/5 increment
    T2=T2+inc/5;
    % Run ODE
    [t,y]=ode45(@Dimensionless_Damped_Bellows_On_Off_ODE,[0 ts],...
          [X0 Xd0(iX) P0 P0],[optODE],M,K,Kb,G,n,V10,S,B,T1,T2);
    X=  y(:,1);
    % Set prior integration to current
    intp=intc;
    % Calculate new current integration
    intc=trapz(t,abs(X-Xss));
    % Test for integration not improving
    if intc>intp, break, end
    end

    % Update solutions
    sol(iX,:)=[Xd0(iX) T1 T2]
end
```

```
%% Plotting
figure('Position',[0 0 1000 1000])
hold all
ftsz=36;
set(0,'DefaultTextInterpreter', 'latex')
plot([0 ts],[Xss Xss],'g-.','LineWidth',3)
plot([0 ts],[-B*V10 -B*V10],'r-.','LineWidth',3)

for i=1:length(sol)
    [t,y]=ode45(@Dimensionless_Damped_Bellows_Adapt_ODE,[0 ts],...
          [X0 sol(i,1) P0 P0],[],M,K,Kb,G,n,V10,S,B,sol(i,2),sol(i,3));
    X=y(:,1);
    plot(t,X,'k','LineWidth',2)
    [~,it]=min(abs(sol(i,2)-t));
    plot(sol(i,2),X(it),'k.','markersize', 30)
end

xlabel('Time T','FontSize',ftsz);
ylabel('Displacement X','FontSize',ftsz)
set(gca,'FontSize',ftsz)
```

E.2 MATLAB: Dimensionless_Damped_Bellows_On_Off_ODE.m

```
function dx=Dimensionless_Damped_Bellows_On_Off_ODE(T,x,M,K,Kb,G,n,V10,S,B,T0,T1)
% John Trautwein jktrautwein@gmail.com  2015/10/14
% ODE using On/Off control with T1 and T2

    dx=zeros(4,1);%This is a pre-initialization.
```

```
V2 = 1-V10;
X=x(1);
Xd=x(2);
P1 = x(3);
P2 = x(4);

% Valve Closed
if T0<T && T<T1
    S=0;
end

% Check for Choked Flow
Pu=max([P1 P2]);
Pd=min([P1 P2]);

if Pu/Pd > ((n+1)/2)^(n/(n-1))
    C2= sqrt(n/(((n+1)/2 )^((n+1)/(n-1))));
else
    C2= (Pd/Pu)^(1/n)*sqrt((2*n/(n-1))*(1-(Pd/Pu)^((n-1)/n)));
end

% Contact Base Input
if X<=0
   D=X;
   Dd=Xd;
else
   D=0;
   Dd=0;
end
```

```
    % Equation of Motion
    Xdd = ((X<=0)*(P1-K*D)-(X<=-B*V10)*Kb*(B*V10+D)-M*G)/M;

    % Differential Equations of Pressure
    if P2>P1
       P1d=(C2*S*P1^((n-1)/n)*P2^((n+1)/(2*n))-n*Dd*P1)/(V10+D);
       P2d= -C2*S*P2^((3*n-1)/(2*n))/V2;
    else
       P1d=(-C2*S*P1^((3*n-1)/(2*n))-n*Dd*P1)/(V10+D);
       P2d= C2*S*P2^((n-1)/n)*P1^((n+1)/(2*n))/V2;
    end

    % Differentials
    dx(1)=Xd;
    dx(2)=Xdd;
    dx(3)=P1d;
    dx(4)=P2d;

end
```

E.3 MATLAB: Active_P0_V10_Finder.m

```
% John Trautwein jktrautwein@gmail.com  2015/10/14
% Contour plot for solutions to Upper Stroke Limits > Bottom

clear all;
close all;

% System non dimensional Parameters
```

```
n=  1.4;    % Ratio of specific heats
M=  1;      % Moving Mass
B=  .95;    % Bellows Ratio (effective area/cylinder area)
G=  1;      % Gravity
K=  0;      % Bellows Stiffness
X0= 0;      % Position
Xd0=-1;     % Max Velocity

% Test Range for P0 and V10
P0=.3:.01:.8;
V10=.1:.01:.6;

opt = optimset('Display','off');

% Preallocate
sol=zeros(length(P0),length(V10));

% Loop over iP and iV
for iP=1:length(P0)
for iV=1:length(V10)

% Steadt State Calculation
SteadyState=@(Dv)P0(iP)./(1+Dv).^n-K.*Dv-M*G;

% Calculate Stroke Limits
% Change in Kinetic Energy
KE=1/2*M*Xd0^2;
% Change in Potential Gravitational Energy
PE=@(Dv)M*G*(X0-Dv);
% Change in Potential Spring Energy
SE=@(Dv)1/2*K*Dv.^2;
```

```
% Compression work for upper limit
PWu=@(Dv)(P0(iP)*V10(iV)^n/(1-n))*((V10(iV)+Dv).^(1-n)-V10(iV)^(1-n));
% Solve for Stroke Limits
Xsu=fzero(@(Dv) KE+PE(Dv)-SE(Dv)+PWu(Dv),-V10(iV)/2,opt);
% Solve for Steady State
Xss=fzero(SteadyState,-V10(iV)/2);
% Solve for Bottom
Xbt=-B*V10(iV);

% Create Solution that meets critera
sol(iP,iV)=(Xsu-Xbt)*(Xss<Xbt && Xsu>Xbt);

end
end

%%

% Create Contour Plot
ftsz=36;
figure('Position',[0 0 1000 1000])
hold all

[C, H]=contourf(P0,V10,sol');
set (H, 'LineWidth',0.1);
colorbar('northoutside');
xlabel('$P_0$','FontSize',ftsz)
ylabel('$V_{10}$','FontSize',ftsz)

set(0,'DefaultTextInterpreter', 'latex')

% Change background color to white
```

```
myColorMap = jet; % Make a copy of jet.
myColorMap(1, :) = [1 1 1];
colormap(myColorMap); % Apply the colormap
set(gca,'FontSize',ftsz)

% Plot X at maximum point
[pmax,vmax]= find(sol==max(sol(:)));
plot(P0(pmax),V10(vmax),'kx','MarkerSize',30,'Linewidth',8)
plot(P0(pmax),V10(vmax),'x','MarkerSize',26,'Linewidth',4,'Color',[1 1 1])
```

E.4 MATLAB: Min_T1_Find.m

```
function F=Min_T1_Find(T1,X0,Xd0,P0,M,K,Kb,G,n,V10,S,B)
% John Trautwein jktrautwein@gmail.com  2015/10/14
% Use to find T1 and return difference with minimum of X

% Time of Simulation set to one period
ts=inv((1/2/pi)*sqrt((n*P0/V10+K)/M));

T2= ts; % Valve Open Time

SteadyState=@(Dv)P0./(1+Dv).^n-K.*Dv-M*G;
Xss=fzero(SteadyState,-V10/2);

% Run ODE
opt = odeset('RelTol',1e-14);
[~,y]=ode45(@Dimensionless_Damped_Bellows_On_Off_ODE,[0 ts],...
    [X0 Xd0 P0 P0],[opt],M,K,Kb,G,n,V10,S,B,T1,T2);
```

```
X=  y(:,1);


% Function Return
F=min(X)-Xss;


end
```

APPENDIX F: OPTIMIZATION

F.1 MATLAB: Nondimensional_Optimization_Nonlin_Obj.m

```
% John Trautwein jktrautwein@gmail.com  2015/10/14
% Find Optimum Parameters for S, V10, K, P0 to maximize damping ratio
clear all;
close all;

% System non dimensional Parameters
n=1.4;  % Ratio of specific heats

% Fixed Paramters
M= 1;   % Moving Mass
G= 1;    % Gravity
Kb=1e6; % Bellows Bottom Out Stiffness
X0= 0; %  Initial Position
Xd0= -1; % Initial Velocity
T0= 0; % Valve Open Time
C=  1;     % Check Valve %S
B=  .9; % Bellows Ratio (effective area/cylinder area)

S=  .1:.05:.5; % Orifice Ratio (orifice area/cilinder area)
V10=.3:.05:.6; % Volume Ratio (Initial Volume 1/Total Initial Volume)
K=  0:.1:1;  % Bellows Stiffness
P0= .5:.05:.9;   % Initial Pressure

iSn=length(S);
iVn=length(V10);
iKn=length(K);
iPn=length(P0);
```

```
sol=ones(1,7);
soli=2;

%% Loops

for iS=1:iSn
for iV=1:iVn
for iK=1:iKn
for iP=1:iPn
    % Period of one cycle estimate
    ts=inv((1/2/pi)*sqrt((n*P0(iP)/V10(iV)+K(iK))/M));
    % Run ODE for 2 cycles
    options = odeset('RelTol',1e-14);
    [t,y]=ode45(@Dimensionless_Damped_Bellows_ODE,[0 2*ts],...
         [X0 Xd0 P0(iP) P0(iP)],[],M,K(iK),Kb,G,n,V10(iV),S(iS),T0,B,C);
    X=  y(:,1);
    % Criteria and Objective Function
    c1=(min(real(X))>-B*V10(iV));
    c2=(max(real(X))<=0);

    if c1&&c2
       % Run for 10 cyles to get damping ratio
       [t,y]=ode45(@Dimensionless_Damped_Bellows_ODE,[0 10*ts],...
       [X0 Xd0 P0(iP) P0(iP)],[],M,K(iK),Kb,G,n,V10(iV),S(iS),T0,B,C);
       X=y(:,1);
       % Steady State Calculation
       SteadyState=@(Dv)P0(iP)./(1+Dv).^n-K(iK).*Dv-M*G;
       Xss=fzero(SteadyState,-B*V10(iV)/2);
       % Damping Model
       modelFun=@(b,t) cumtrapz(t,b(1)*exp(-b(2)*t)+b(3));
```

```
        % Numerically Integrate Data
        sum=cumtrapz(t,abs(X-Xss));
        start = [.1 .1 .1];
        % Fit Model to Data
        nlm = fitnlm(t,sum,modelFun,start);
        % Save results to output
        sol(soli,:)=[iS iV iK iP nlm.Coefficients.Estimate(1) ...
                                 nlm.Coefficients.Estimate(3) ...
                                 nlm.Coefficients.Estimate(2)];
        % Index solution
        soli=soli+1;
    end

end
end
% Set up Time Status
clc
percom=((iS-1)*iVn*iKn*iPn+(iV-1)*iKn*iPn+(iK-1)*iPn+(iP-1))...
    /(iSn*iVn*iKn*iPn);
fprintf('%3.0f percent complete: %4.2f min remaining \n',...
    100*percom,toc/60/percom-toc/60)
end
end


%% Finding Optimum Solutions

sol=sortrows(sol(2:end,:),[-7]);


%% Plotting First Two Solutions
```

```
set(0, 'DefaultAxesFontSize',36);
set(0,'DefaultTextInterpreter', 'latex')
close all
Var_Names = {'S' 'V_10' 'K' 'P' 'A' 'B' 'zeta'};

% Solutions to compare in plots
comp=[1 5];

T = table(S(sol(comp,1))',V10(sol(comp,2))',K(sol(comp,3))'...
          ,P0(sol(comp,4))',sol(comp,5),...
           sol(comp,6),sol(comp,7),'VariableNames',Var_Names')

ftsz=36;
LinSt={'-', '--', ':', '--'};
LinCl={'b','r','g','r'};
figure('Position',[0 0 1000 1000])
figure('Position',[0 0 1000 1000])
figure('Position',[0 0 1000 1000])
figure('Position',[0 0 1000 1000])


% Calculate Optimal Solution
ilin=1;
for iplot=1:length(comp)

iS=sol(comp(iplot),1);
iV=sol(comp(iplot),2);
iK=sol(comp(iplot),3);
iP=sol(comp(iplot),4);

    % Parameters update for new Solution
```

```
opt = odeset('RelTol',1e-14);
[t,y]=ode45(@Dimensionless_Damped_Bellows_ODE,[0 10*ts],...
    [X0 Xd0 P0(iP) P0(iP)],[opt],M,K(iK),Kb,G,n,V10(iV),S(iS),T0,B,C);

X=  y(:,1);
Xd= y(:,2);
P1= y(:,3);

D=nan(length(X),1);
Dd=nan(length(X),1);

  for j=1:length(X)
    if X(j)<0
       D(j)=X(j);
       Dd(j)=Xd(j);
    else
       D(j)=0;
       Dd(j)=0;
    end

  end

% Calculate Accelerations
Xdd = ((X<=0).*(P1-K(iK).*D)-(X<=-B*V10(iV)).*Kb.*(B*V10(iV)+D)-M.*G)./M;

      SteadyState=@(Dv)P0(iP)./(1+Dv).^n-K(iK).*Dv-M*G;
      modelFun=@(b,t) cumtrapz(t,b(1)*(exp(-b(2)*t)+b(3)));
      Xss=fzero(SteadyState,-B*V10(iV)/2);
      sum=cumtrapz(t,abs(X-Xss));
      start = [.1 .1 .1];
      nlm = fitnlm(t,sum,modelFun,start);
```

```
      b=nlm.Coefficients.Estimate;
      XSS(ilin)=Xss;

figure(1)
    hold all
    plot(t,X,'LineWidth',2,'Color',LinCl{ilin},'LineStyle',LinSt{ilin})
    plot(t,Xss-pi/2*b(1)*(exp(-b(2)*t)+b(3)),...
        'LineWidth',2,'Color',LinCl{ilin},'LineStyle',...
        '-.','handlevisibility','off')

figure(2)
    hold all
    plot(t,abs(Xd),'LineWidth',2,'Color',LinCl{ilin},...
        'LineStyle',LinSt{ilin})

figure(3)
    hold all
    plot(t,Xdd,'LineWidth',2,'Color',LinCl{ilin},'LineStyle',LinSt{ilin})

figure(4)
    hold all
    plot(X,Xd,'LineWidth',2,'Color',LinCl{ilin},'LineStyle',LinSt{ilin})

ilin=ilin+1
end

%% Plot Configuration

figure(1)
    xlabel('Time, T','FontSize',ftsz);
    ylabel('Displacement X','FontSize',ftsz)
```

```
    axis([0 20 -.6 .1])
    set(gca,'XTick',[0 5 10 15 20])
    set(gca,'YTick',[-.5 -.25 0])
    set(gca,'FontSize',ftsz)
    Leg_st=legend(strcat('$\zeta=$',num2str(sol(comp,7),3)));
    h= legend(Leg_st);
    set(h,'Interpreter','latex')

figure(2)
    hold all
    xlabel('Time T','FontSize',ftsz);
    ylabel('Velocity $\dot{X}$','FontSize',ftsz)
    axis([0 10 -1 1])
    set(gca,'FontSize',ftsz)
    Leg_st=legend(strcat('$\zeta=$',num2str(sol(comp,7),3)));
    h= legend(Leg_st);
    set(h,'Interpreter','latex')

figure(3)
    hold all
    xlabel('Time T','FontSize',ftsz);
    ylabel('Acceleration $\ddot{X}$','FontSize',ftsz)
    axis([0 20 -1 8])
    set(gca,'XTick',[0 5 10 15 20])
    set(gca,'FontSize',ftsz)
    Leg_st=legend(strcat('$\zeta=$',num2str(sol(comp,7),3)));
    h= legend(Leg_st);
    set(h,'Interpreter','latex')

figure(4)
   hold all
```

```
    ylabel('Velocity $\dot{X}$','FontSize',ftsz);
    xlabel('Displacement $X$','FontSize',ftsz)
    axis([-.5 0 -1 .6 ])
    set(gca,'XTick',[-.50 -.25  0])
    set(gca,'YTick',[-1 -.5 0 .5 1])
    Leg_st=legend(strcat('$\zeta=$',num2str(sol(comp,7),3)));
    h= legend(Leg_st);
    set(h,'Interpreter','latex')

    for i=length(comp)
        plot([XSS(i) XSS(i)],[-1 1],'LineWidth',2,'Color',...
            LinCl{i},'LineStyle','-.','handlevisibility','off')
    end
```

F.2 MATLAB: Bellows_initial_sizing_nonlin_Opt.m

```
% John Trautwein jktrautwein@gmail.com  2015/10/14
% Find lightest COTS Bellows Length of each size that meets goal
clear all
close all
set(0, 'DefaultAxesFontSize',36);
set(0,'DefaultTextInterpreter', 'latex')

filename = 'bellows_data.csv';
[num] = csvread(filename,2,0);

% Data Input
ro=num(:,3)/2/1000; % (m) Outside Radius m
ri=num(:,4)/2/1000; % (m) Inside Radius m
```

```
Ae=pi/3*(ro.^2+ro.*ri+ri.^2); % (m^2) Effective Area m^2
Ae2=pi/4*(ro.^2+2*ro.*ri+ri.^2); % (m^2) Efffective Area Vendor Calc
Aed=num(:,5)*100/1e6; % (m^2) Effective Area Vendor Data
Pmax=num(:,6)*1000; % (Pa) Max Pressure
Ls_c=num(:,7)/1000; % (m) Stroke per Capsule
Lf_c=num(:,8)/1000; % (m) Free Length per Capsule
Lc_c=num(:,9)/1000; % (m) Compressed Length per Capsule
kb_c=num(:,10)/1000; % (N/m) Spring Rate per Capsule

% Given Problem Data
g=9.8/6; % (m/s^2) Gravitational Acceleration
n=1.4; % (1) Gas Constant
m=100; % (kg) Payload Mass
xd0=1; % (m/s) Initial velocity at ground contact
x0=0;  % (m) Intial heigh above ground contact
R=288; % (J/kg) Gas Constant
theta=300; % (K)
C0=.7; % Discharge Coeffficient

cd= 7:12;       % Diameter Code (row number in table)
N=  15:35;      % Number of capsules
V10=.1:.05:.3;  % Volume Ratio (Initial Volume 1/Total Initial Volume)
P0= .1:.05:.5;  % Initial Pressure
S=  .1:.05:.7;   % Orifice Ratio (orifice area/cilinder area)

% Set Constant Nondimensional Parameters
Kb=1e6;     % Bottoming Sitffness
C=1;        % No Check Valve
T0=0;       % No Valve Dealy
Xd0=-1;     % Initial Velocity (Always -1 due to xd0 being
            %  reference velocity)
```

```
% Set loop lengths
icdn=length(cd);
iNn=length(N);
iVn=length(V10);
iPn=length(P0);
iSn=length(S);

% Set Status Display
Var_Names = {'ID' 'Capsules' 'V_10' 'P_0' 'S' ...
             'zeta' 'mass'};
sol=ones(1,7);
soli=2;
iS=1;
tic
% Loop over cd and number of capsules

%%

for icd=1:icdn
    sc=ro(cd(icd))^2*pi;    % Cylinder Area
    s=Aed(cd(icd));         % Effective Area
    B=s/sc;                 % Bellows Area Ratio
    p10=Pmax(cd(icd));      % Allowable Pressure used for scaling
                            % max nondimensional pressure = 1
    fbreak=0;               % Used to break out of loops once solution found

for iN=1:iNn;
    ls=Ls_c(cd(icd))*N(iN); % Stroke Length
    k=kb_c(cd(icd))/N(iN);  % Spring Rate
    mass=8000*pi*(ro(cd(icd)).^2-ri(cd(icd)).^2).*Lc_c(cd(icd)).*N(iN);
```

```
for iV=1:iVn
    l=sc*ls/V10(iV)/s;      % Simplified Cylinder length
    X0=x0/l;                % Non Dim Initial Height
    M=m*xd0^2/(p10*s*l);    % Non Dim Mass
    K=k*l/p10/xd0;          % Non Dim Stiffness
    G=g*l/xd0^2;            % Non Dim Gravity

for iP=1:iPn
    clc
    [cd(icd) N(iN) iV iP iS]
    % Energy Equation used as time saver to only fun ODE when a solution
    % doesn't bottom out
    % Calculate Stroke Limits
    % Change in Kinetic Energy
    KE=1/2*M*Xd0^2;
    % Change in Potential Gravitational Energy
    PE=@(Dv)M*G*(X0-Dv);
    % Change in Potential Spring Energy
    SE=@(Dv)1/2*K*Dv.^2;
    % Compression work for upper limit
    PWu=@(Dv)(P0(iP)*V10(iV)^n/(1-n))*((V10(iV)+Dv).^(1-n)-V10(iV)^(1-n));
    % Energy at Upper Stroke Limit
    Eu=@(Dv) KE+PE(Dv)-SE(Dv)+PWu(Dv);

    % Energy when bottomed. Will be negative if cylinder won't bottom out
    % May also produce complex solutions which need to be handled.
    Eut=Eu(-B*V10(iV));

    if Eut*isreal(Eut)<0
```

```
for iS=1:iSn


% Period of one cycle estimate
ts=inv((1/2/pi)*sqrt((n*P0(iP)/V10(iV)+K)/M));
% Run ODE for 2 cycles
[t,y]=ode45(@Dimensionless_Damped_Bellows_ODE,[0 2*ts],...
    [X0 Xd0 P0(iP) P0(iP)],[],M,K,Kb,G,n,V10(iV),S(iS),T0,B,C);

X=y(:,1);
P1=y(:,3);

% Check Criteria
c1=(max(t)==2*ts);
c2=(min(real(X))>-B*V10(iV));
c3=(max(real(X))<=0);
c4=(max(P1)<=1);

if c1&&c2&&c3&&c4
   % Run for 10 cycles to get damping ratio
   [t,y]=ode45(@Dimensionless_Damped_Bellows_ODE,[0 10*ts],...
         [X0 Xd0 P0(iP) P0(iP)],[],M,K,Kb,G,n,V10(iV),S(iS),T0,B,C);
   X=y(:,1);
   % Steady State Calculation
   SteadyState=@(Dv)P0(iP)./(1+Dv).^n-K.*Dv-M*G;
   Xss=fzero(SteadyState,-B*V10(iV)/2);
   % Damping Model
   modelFun=@(b,t) cumtrapz(t,b(1)*(exp(-b(2)*t)+b(3)));
   % Numerically Integrate Data
   sum=cumtrapz(t,abs(X-Xss));
   start = [.1 .1 .1];
```

```
        % Fit Model to Data
        nlm = fitnlm(t,sum,modelFun,start);
        % Save results to output
        sol(soli,:)=[icd iN iV iP iS nlm.Coefficients.Estimate(2) mass]
        % Index solution
        soli=soli+1;
        fbreak=1;
    end
    % Break from iS loop
    if fbreak==1
        break;
    end
    end
    %------------------
    end
    % Break from iP loop
    if fbreak==1
        break;
    end
end
    %------------------
    % Break from iV loop
    if fbreak==1
        break;
    end
end
%------------------
    % Break from iN loop
    % Comment out if want several N for each id
    if fbreak==1
        break;
```

```
    end
end
%----------------------
end

% Sort by mass and remove header row
sol=sortrows(sol(2:end,:),[7 -6]);

%% Plot Results
close all

T = table(cd(sol(:,1))',N(sol(:,2))',V10(sol(:,3))',...
          P0(sol(:,4))',S(sol(:,5))',sol(:,6),sol(:,7),...
          'VariableNames',Var_Names')
ftsz=36;
LinSt={'-', '--', ':', '--'};
LinCl={'b','r','g','r'};
figure('Position',[0 0 1000 1000])
figure('Position',[0 0 1000 1000])
figure('Position',[0 0 1000 1000])
figure('Position',[0 0 1000 1000])

comp=[1 2];
% Plot first two solutions
for iplot=1:length(comp)

icd=sol(comp(iplot),1);
iN=sol(comp(iplot),2);
iV=sol(comp(iplot),3);
iP=sol(comp(iplot),4);
iS=sol(comp(iplot),5);
```

```
% Parameters update for new Solution
sc=ro(cd(icd))^2*pi;
s=Aed(cd(icd));
p10=Pmax(cd(icd));
ls=Ls_c(cd(icd))*N(iN);
l=sc*ls/V10(iV)/s;
k=kb_c(cd(icd))/N(iN);
K=k*l/p10/xd0;
B=s/sc;
M=m*xd0^2/(p10*s*l);
G=g*l/xd0^2;
Tp=2*pi*sqrt(M*V10(iV)/n/P0(iP));
ts=5*Tp;



opt = odeset('RelTol',1e-14);
[t,y]=ode45(@Dimensionless_Damped_Bellows_ODE,[0 20],...
    [X0 Xd0 P0(iP) P0(iP)],[opt],M,K,Kb,G,n,V10(iV),S(iS),T0,B,C);


X=  y(:,1);
Xd= y(:,2);
P1= y(:,3);


D=nan(length(X),1);
Dd=nan(length(X),1);


  for j=1:length(X)
    if X(j)<0
       D(j)=X(j);
```

```
        Dd(j)=Xd(j);
    else
        D(j)=0;
        Dd(j)=0;
    end

  end

% Calculate Accelerations
Xdd = ((X<=0).*(P1-K.*D)-(X<=-B*V10(iV)).*Kb.*(B*V10(iV)+D)-M.*G)./M;

      SteadyState=@(Dv)P0(iP)./(1+Dv).^n-K.*Dv-M*G;
      modelFun=@(b,t) cumtrapz(t,b(1)*(exp(-b(2)*t)+b(3)));
      Xss=fzero(SteadyState,-B*V10(iV)/2);
      sum=cumtrapz(t,abs(X-Xss));
      start = [.1 .1 .1];
      nlm = fitnlm(t,sum,modelFun,start);
      b=nlm.Coefficients.Estimate;
      XSS(comp(iplot))=Xss;

figure(1)
    hold all
    plot(t,X,'LineWidth',2,'Color',LinCl{comp(iplot)},...
        'LineStyle',LinSt{comp(iplot)})
    plot(t,Xss-pi/2*b(1)*(exp(-b(2)*t)+b(3)),...
        'LineWidth',2,'Color',LinCl{comp(iplot)},...
        'LineStyle','-.','handlevisibility','off')

figure(2)
    hold all
    plot(t,abs(Xd),'LineWidth',2,'Color',LinCl{comp(iplot)},...
```

```
        'LineStyle',LinSt{comp(iplot)})

figure(3)
    hold all
    plot(t,Xdd,'LineWidth',2,'Color',LinCl{comp(iplot)},...
        'LineStyle',LinSt{comp(iplot)})

figure(4)
    hold all
    plot(X,Xd,'LineWidth',2,'Color',LinCl{comp(iplot)},...
        'LineStyle',LinSt{comp(iplot)})
end

%% Plot Configuration

figure(1)
    xlabel('Time, T','FontSize',ftsz);
    ylabel('Displacement X','FontSize',ftsz)
    axis([0 5 -.15 0])
    set(gca,'XTick',[0 1 2 3 4 5])
    set(gca,'YTick',[-.15 -.1  -.05 0 .05])
    set(gca,'FontSize',ftsz)
    Leg_st=legend(strcat('$\zeta=$',num2str(sol(1,6),2))...
             ,strcat('$\zeta=$',num2str( sol(2,6),3 )) );
    h= legend(Leg_st);
    set(h,'Interpreter','latex')

figure(2)
    hold all
    xlabel('Time T','FontSize',ftsz);
    ylabel('Velocity $\dot{X}$','FontSize',ftsz)
```

```
    axis([0 10 -1 1])
    set(gca,'FontSize',ftsz)
    Leg_st=legend(strcat('$\zeta=$',num2str(sol(1,6),2))...
             ,strcat('$\zeta=$',num2str( sol(2,6),3 )) );
    h= legend(Leg_st);
    set(h,'Interpreter','latex')

figure(3)
    hold all
    xlabel('Time T','FontSize',ftsz);
    ylabel('Acceleration $\ddot{X}$','FontSize',ftsz)
    axis([0 5 -4 12])
    set(gca,'XTick',[0 1 2  3 4  5])
    set(gca,'FontSize',ftsz)
    Leg_st=legend(strcat('$\zeta=$',num2str(sol(1,6),2))...
             ,strcat('$\zeta=$',num2str( sol(2,6),3 )) );
    h= legend(Leg_st);
    set(h,'Interpreter','latex')

figure(4)
   hold all
   ylabel('Velocity $\dot{X}$','FontSize',ftsz);
   xlabel('Displacement $X$','FontSize',ftsz)
   axis([-.125 0 -1 1 ])
   set(gca,'XTick',[-.1  -.050  0])
   set(gca,'YTick',[-1 -.5 0 .5 1])
   set(gca,'FontSize',ftsz)
    Leg_st=legend(strcat('$\zeta=$',num2str(sol(1,6),2))...
             ,strcat('$\zeta=$',num2str( sol(2,6),3 )) );
    h= legend(Leg_st);
    set(h,'Interpreter','latex')
```

```
for i=[1 2]
    plot([XSS(i) XSS(i)],[-1 1],'LineWidth',2,'Color',...
        LinCl{i},'LineStyle','-.','handlevisibility','off')
end
```

Table F.1: bellows_data.csv

Code	D_o	D_i	A_e	P_{max}	per capsule			
					L_s	L_{max}	L_{min}	k_b
	mm	mm	cm^2	KPa	mm	mm	mm	N/mm
5	9.5	3.2	0.3	689	3.6	5.3	1.8	2.3
10	12.7	4.8	0.6	1034	8.4	11.7	3.3	9.6
20	19.0	6.4	1.3	345	7.6	9.9	2.3	4.2
30	26.2	14.0	3.2	207	13.5	16.8	3.3	4.4
35	38.1	24.6	7.7	276	7.4	10.9	3.6	3.9
40	41.4	19.0	7.1	297	7.9	10.9	3.0	2.1
50	48.0	35.3	13.6	310	21.8	26.7	4.8	2.6
55	57.2	38.1	17.7	345	12.7	18.3	5.6	3.7
60	64.8	44.4	23.4	345	18.0	24.6	6.6	4.7
70	75.9	50.8	31.6	276	23.9	29.7	5.8	5.1
80	101.3	68.3	56.5	276	25.4	31.8	6.4	8.8
85	108.0	81.3	71.0	310	20.3	28.7	8.4	13.1
90	126.2	101.6	101.9	345	20.3	29.2	8.9	13.1
93	177.3	126.5	181.3	172	25.4	30.2	4.8	7.4
95	279.4	241.3	532.1	138	25.4	29.0	3.6	43.8
98	457.2	406.4	1463.9	138	25.4	29.7	4.3	113.8

LIST OF REFERENCES

[1] Blaine W Andersen. *The analysis and design of pneumatic systems*. Krieger Pub. Co, 1967.

[2] Manned Spacecraft. Space explorers. 2(6), 2004.

[3] NASA. *Mars Exploration Rover - Spirit*, (accessed October 29, 2015).

[4] http://bananasaboutcars.com/. *Hydraulic Shock Schematic*, (accessed September 7, 2015).

[5] George A Zupp. An analysis and a historical review of the apollo program lunar module touchdown dynamics. 2013.

[6] Manned Spacecraft. 7th aerospace mechanisms symposium. 1972.

[7] William F Rogers. Apollo lunar module landing gear. *NASA Technical Memorandum*, (58106):123, 1972.

[8] Stephan Ulamec, Vladimir Kucherenko, Jens Biele, Alexei Bogatchev, A Makurin, and S Matrossov. Hopper concepts for small body landers. *Advances in Space Research*, 47(3):428–439, 2011.

[9] cyberneticzoo.com. Phobos hopper, (accessed September 23 , 2015).

[10] Tetsuo Yoshimitsu, Takashi Kubota, and Ichiro Nakatani. Minerva rover which became a small artificial solar satellite. 2006.

[11] M. Hilchenbach. Simulation of the landing of rosetta philae on comet 67p/churyumov-gerasimenko. In *SIMPACK User Meeting, 2004*. Max-Planck-Institut für Sonnensystemforschung, 2004.

[12] ATG MediaLab ESA. *Philae Lander*, (accessed August 7, 2015).

[13] Sarah L Nothnagel, Zachary J Bailey, Phillip M Cunio, Jeffrey A Hoffman, Babak E Cohanim, and Brett J Streetman. Development of a cold gas spacecraft emulator system for the talaris hopper. In *AIAA SPACE 2010 Conference & Exposition*, page 8778, 2010.

[14] Sarah Lynn Nothnagel. Development of a cold gas propulsion system for the talaris hopper. 2011.

[15] Stefaan Duym, Randy Stiens, and Koenraad Reybrouck. Evaluation of shock absorber models. *Vehicle system dynamics*, 27(2):109–127, 1997.

[16] Qiang Wang, Mehdi Ahmadian, and Zhaobo Chen. A novel double-piston magnetorheological damper for space truss structures vibration suppression. *Shock and Vibration*, 2014, 2014.

[17] YT Wang, R Singh, HC Yu, and DA Guenther. Computer simulation of a shock-absorbing pneumatic cylinder. *Journal of Sound and vibration*, 93(3):353–364, 1984.

[18] YT Wang, R Singh, and DA Guenther. Modeling of an impulse-absorbing pneumatic cylinder. *Journal of Sound and Vibration*, 82(4):598–600, 1982.

[19] J-C Maré, O Geider, and S Colin. An improved dynamic model of pneumatic actuators. *International Journal of Fluid Power*, 1(2):39–49, 2000.

[20] R Palej, S Piotrowski, and M Stojek. Mechanical properties of an active pneumatic spring. *Journal of sound and vibration*, 168(2):299–306, 1993.

[21] Huayan Pu, Xin Luo, and Xuedong Chen. Modeling and analysis of dual-chamber pneumatic spring with adjustable damping for precision vibration isolation. *Journal of Sound and Vibration*, 330(15):3578–3590, 2011.

[22] Nathalal Gordhanbhai Patel. Linear analysis of pneumatic dashpot damping. 1970.

[23] RL Peskin and E Martinez. A study of the response of a small porous chamber to forced oscillation. *Journal of Fluids Engineering*, 88(1):25–32, 1966.

[24] MS Hundal. Passive pneumatic shock isolator: analysis and design. *Journal of Sound and Vibration*, 84(1):1–9, 1982.

[25] MS Hundal. Shock response of a symmetric pneumatic spring to a velocity pulse. *Journal of Sound and Vibration*, 101(1):33–40, 1985.

[26] MS Hundal. Response of shock isolators with linear and quadratic damping. *Journal of Sound and Vibration*, 76(2):273–281, 1981.

[27] Mahendra S Hundal and VT Burlington. Damped pneumatic spring as shock isolator: generalized analysis and design procedure. *Shock Vib Bull*, 53:161–168, 1983.

[28] MS Hundal. Analysis of performance of pneumatic impact absorbers. *Journal of Mechanical Design*, 100(2):236–241, 1978.

[29] Y Ooka, H Ogawa, K Ohno, and K Dozaki. Simulative analyses of dynamic buckling of bellows. *Journal of pressure vessel technology*, 118(2):129–136, 1996.

[30] Hyspan Precision Products. Pressure thrust, 1986 (accessed April 7, 2uu015).

[31] Senior Aerospace. *OTS Bellows*, (accessed April 7, 2015).

[32] R Wiszowaty, J Biczyk, C Graczykowski, and G Mikułowski. Method of impact energy dissipation by the use of the pneumatic impact absorber with a piezo-valve. In *Proc. 5th ECCOMAS Thematic Conference on Smart Structures and Materials SMART'11*, pages 6–8, 2011.

[33] Grzegorz Mikułowski, Rafał Wiszowaty, and Jan Holnicki-Szulc. Characterization of a piezoelectric valve for an adaptive pneumatic shock absorber. *Smart Materials and Structures*, 22(12):125011, 2013.

[34] Jeff Hass. personal communication, 2015-01-16.

[35] FD Ezekiel and HM Paynter. Fluid power transmission. *from" Fluid Power Control," by JF Blackburn, G. Reethof, and Shearer, editors, The Technology Press of MIT and John Wiley & Sons, Inc., New York, N. Y*, pages 139–143, 1960.